THE FORMATION OF NOVEL LAYERED COMPOUNDS BY EXFOLIATION AND RESTACKING OF CADMIUM PHOSPHORUS TRISULPHIDE WITH THE BIOLOGICAL MOLECULES ADENOSINE MONOPHOSPHATE AND CYTIDINE MONOPHOSPHATE INCLUDED

by

Philippe Westreich

B.Sc. Hons., McGill University, 1996

M.Sc., Simon Fraser University, 1998

THESIS SUBMITTED IN PARTIAL FULFILLMENT

OF THE REQUIREMENTS FOR THE DEGREE OF

DOCTOR OF PHILOSOPHY

IN THE DEPARTMENT

OF

PHYSICS

SIMON FRASER UNIVERSITY

Fall 2004

APPROVAL

Name: Philippe Westreich

Degree: Doctor of Philosophy

Title of Thesis: The formation of novel layered compounds by exfoliation and restacking of cadmium phosphorus trisulphide with the biological molecules adenosine monophosphate and cytidine monophosphate included

Examining Committee: Karen Kavanagh, Professor, Dept. of Physics (Chair)

Robert F. Frindt
Professor Emeritus, Dept. of Physics (Senior Supervisor)

John Bechhoefer
Professor, Dept. of Physics

E. Daryl Crozier
Professor Emeritus, Dept. of Physics

Albert E. Curzon
Professor Emeritus, Dept. of Physics

Dipankar Sen
Internal Examiner, Professor, Dept. of Molecular Biology and Biochemistry and Dept. of Chemistry

---

Michael M. Lerner
External Examiner, Professor, Dept. of Chemistry, Oregon State University

Date Approved: November 16, 2004

SIMON FRASER UNIVERSITY

PARTIAL COPYRIGHT LICENCE

Abstract

Exfoliated single layer $Cd_{0.8}PS_3$ has been combined with the biological molecules cytidine monophosphate (CMP) and adenosine monophosphate (AMP) to form the novel restacked compound $Li_xCd_{0.8}PS_3(NMP)_z(H_2O)_y$, where N stands for cytidine or adenosine. Composition was determined using energy dispersive X-ray spectroscopy, and the structure of these compounds was studied using X-ray diffraction on oriented films.

It was found that for the AMP samples, there is little influence of relative humidity (RH) in the range of 0 to 80 %, after which there is a rapid expansion of the interlayer space. In the 0 to 80 % range, for $(AMP)_{0.5}$, a host plane spacing near 19.6 Å was found. Electron density calculations on the X-ray diffraction pattern suggest a model for the arrangement of guest AMP molecules between the host layers, with an accompanying water molecule. The calculations also suggest that there is a buckling in the host layer of about $\pm$ 0.6 Å.

For the $(CMP)_{0.3}$ samples, there is more sensitivity to relative humidity in the 0 - 80 % range, with spacings varying from 20 to 24 Å. Much of this variation is gradual, but at around 50 % RH, there is a discontinous change in the spacing of about 1.8 Å, corresponding to less than the size of a water molecule, that appears to arise from a modification of the CMP conformation.

Possible reasons for the differences in the behaviour of the two systems are explored.

Acknowledgements

I would like to start by thanking my supervisor, Dr. Robert. F. Frindt, for his support and guidance throughout this project. My thanks go out to Dr. Albert Curzon, Dr. Daryl Crozier and Dr. John Bechhoefer for their guidance and helpful suggestions. In addition, I would like to express my gratitude to the above and to Dr. Dipankar Sen and Dr. Michael Lerner for their interest in this project, and for taking the time to read the thesis and provide their comments.

To Dr. Datong Yang, I am very grateful for all the assistance, suggestions and discussions in the lab. My appreciation also goes out to the recently (much too soon) departed Scott Wilson, who provided considerable assistance with the humidity apparatus. Ken Myrtle provided help with the temperamental Siemens diffractometer, and Mehrdad Rastan was a great help with all computer problems that cropped up. Dr. Li Yang and Dr. Karen Kavanagh were of great help with the Energy Dispersive X-ray Spectroscopy, for which I am very appreciative.

Dr. Dan Vernon and Dr. Andrew DeBenedictis were my LaTeX resource people, and also friends who were very generous with their time whenever I needed them.

I would also like to acknowledge the help of the graduate secretaries Candida Mazza and Helen Luk. In addition, Dr. Sada Rangnekar has provided support in all sorts of ways.

The financial support provided by Dr. Frindt through his NSERC grant, and by the SFU physics department through teaching assistant appointments is greatly appreciated.

Finally, I would like to thank my wife Monique and my mother Ruta for their prodding, as well as everyone else who kept asking, "When are you finishing?"

Contents

List of Tables

List of Figures

Chapter 1

Introduction

1.1 Motivation

There has been much recent interest in the encapsulation of biological molecules into layered inorganic host materials [2–10]. In particular, these new materials are being investigated for use as gene reservoirs [2, 3], for gene therapy and drug delivery [2, 4, 5, 9, 10], and for separation processes [6]. While most of these studies have focussed on layered double hydroxides, recently attention has turned to the metal phosphorus trisulfides [7, 8]. For example, Coradin *et al.* [7] have intercalated the cationic biomolecules lysine, poly-lysine and lysozyme into $MnPS_3$ as a first step toward developing materials for biosensing devices.

Nucleoside monophosphates (NMPs) are of particular interest because they form the building blocks of the nucleic acids deoxyribonucleic acid (DNA) and ribonucleic acid (RNA), as well as serving other biological functions. Understanding the change in the structure of the nanocomposites in response to humidity can further our understanding of the NMPs themselves, and may offer insight into the interactions of both these molecules and nucleic acids in general with water.

The layered compound $CdPS_3$ has been shown to exfoliate into single molecular layers, and to encapsulate polymers and other organic molecules by restacking [11], providing an alternative approach to intercalation in the formation of layered nanocomposites. NMPs have been included in layered double hydroxides (LDH) [2, 6], but not in other inorganic host materials. LDH hosts are positively charged, with neg-

atively charged guests included. A review of the intercalation chemistry of LDH is given by Khan and O'Hare [12]. This thesis explores the inclusion of NMPs within metal phosphorus trisulphide (MPS_3) materials for the first time. Unlike LDH systems, the MPS_3 host layers are neutral, or, in the case of restacked $CdPS_3$, they are negatively charged [11].

1.2 $CdPS_3$

$CdPS_3$ is a layered insulating solid from the MPS_3 family, where M is a transition metal. MPS_3 compounds are generally called transition metal phosphorus trisulfides. All of the MPS_3 materials have a similar structure, which is depicted in Figs. 1.1, 1.2 and 1.3. As described by Ouvrard *et al.* [1], the structure belongs to the C2/m space group, with atomic positions as listed in Table 1.1.

Table 1.1: Atomic positions of $CdPS_3$, as listed by Ouvrard *et al* [1], expressed in fractional coordinates.

Atom	x	y	z
Cd	0.0	0.33221(3)	0.0
P	0.0551(2)	0.000	0.1697(2)
S_1	0.7689(2)	0.000	0.2542
S_2	0.2400(1)	0.15659(7)	0.2584(1)

There is a central layer of metal atoms in a hexagonal arrangement (seen most clearly in Fig. 1.2), with the centre of each hexagon containing a pair of phosphorus atoms, displaced 1.1 Å above and below the plane of the Cd atoms. The Cd-P layer is surrounded 1.9 Å above and below by sulphur atoms, coordinated octahedrally to each metal atom or P_2 pair. Successive $CdPS_3$ sandwiches are then displaced from the next along the c-axis to form a monoclinic crystal structure, where the angle β between the a-axis and the c-axis is 107.58°, as shown in Fig. 1.1. The primitive $Cd_2P_2S_6$ unit cell has the following parameters [1]: a = 6.218 Å, b = 10.763 Å, c = 6.867 Å. Since the c-axis is not perpendicular to the layers, it is worth mentioning the perpendicular distance between layers in the crystal, which is just $c \times \sin(107.58°) = 6.546$ Å.

$CdPS_3$ can also be thought of as a salt of Cd^{2+} ions bound to $P_2S_6{}^{4-}$ ions.

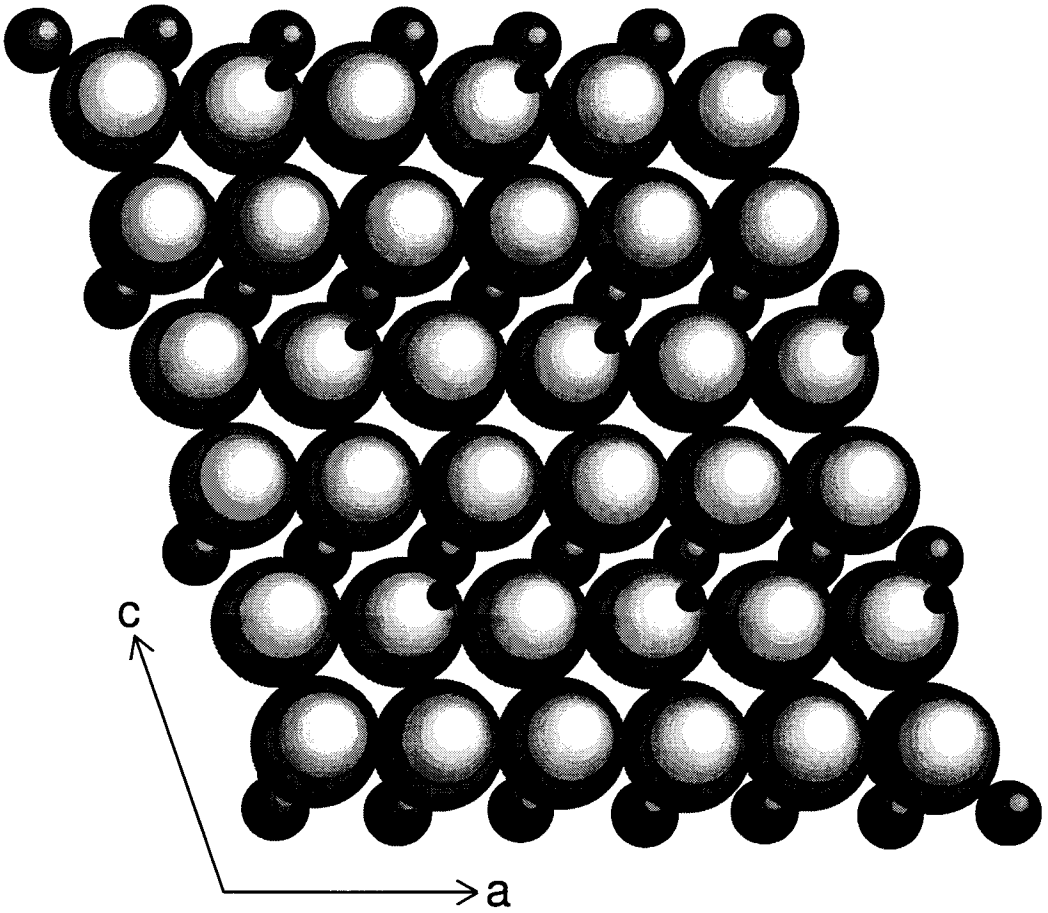

Figure 1.1: Structure of $CdPS_3$: view along the b-axis. Small black spheres represent P atoms, medium gray spheres represent Cd atoms, and large light gray spheres represent S atoms.

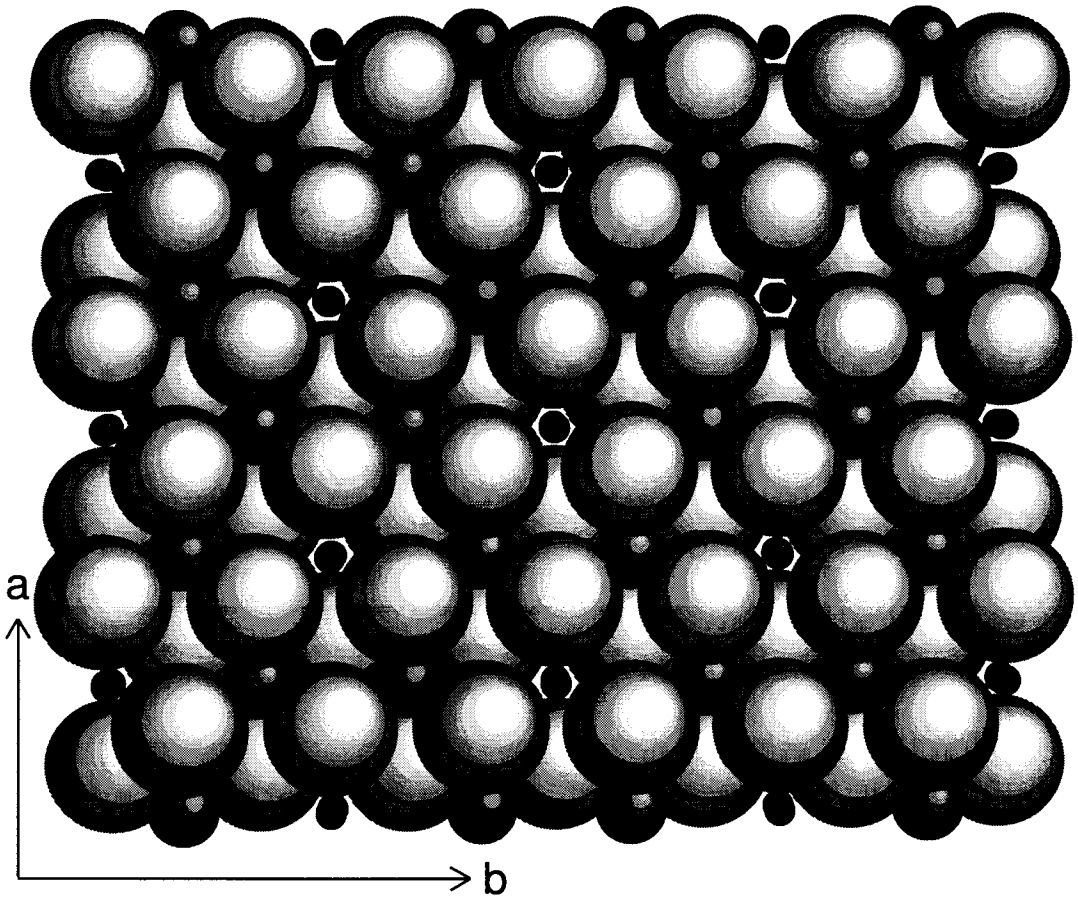

Figure 1.2: A sandwich layer of the $CdPS_3$ structure: view perpendicular to the a-b plane. Small black spheres represent P atoms, medium gray spheres represent Cd atoms, and large light gray spheres represent S atoms.

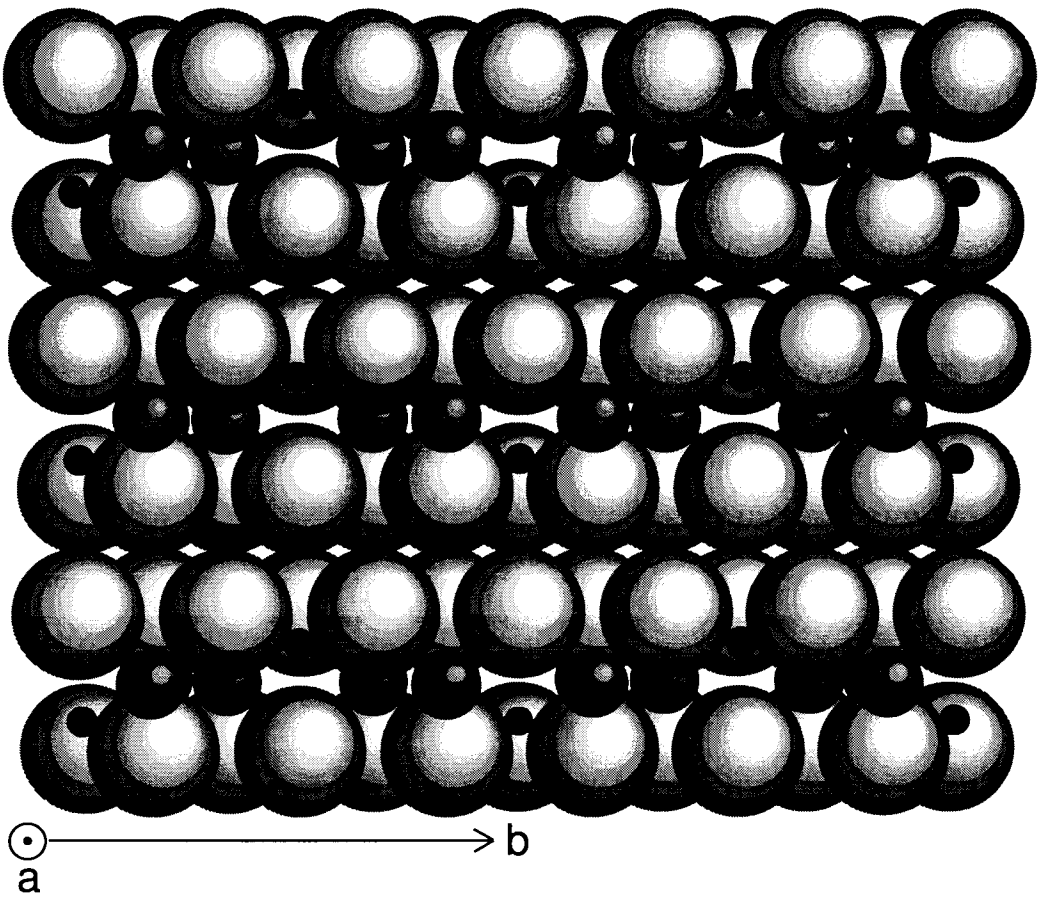

Figure 1.3: Structure of $CdPS_3$: view along the a-axis. Small black spheres represent P atoms, medium gray spheres represent Cd atoms, and large light gray spheres represent S atoms.

MPS_3 materials have been studied primarily for their promising optical and magnetic properties, as well as for their potential as battery electrode materials. They form an attractive class of intercalation compounds, where a wide variety of atoms and molecules have been successfully intercalated directly, or by ion-exchange following alkali metal intercalation. This latter process, first developed by Clément [13], has opened up the intercalation of a large number of cationic and neutral species into $MnPS_3$ and $CdPS_3$ following an initial step of intercalating K^+ ions. Much of the research into intercalation of MPS_3 materials has been summarized in a review by Grasso and Silipigini [14].

An interesting feature of $CdPS_3$ and of some of the other MPS_3s is the formation of metal vacancies upon alkali metal (and other ion) intercalation [13, 15]. The alkali metal ions then become associated to the vacancy sites. There is some debate as to whether these vacancies are ordered [16–18]. Fig. 1.4 illustrates the Cd-P layer for a random array of 1/5 Cd vacancies. One fifth is the approximate ratio of vacancies to original Cd positions upon alkali metal intercalation, though it can range from 1/6 to 1/4.

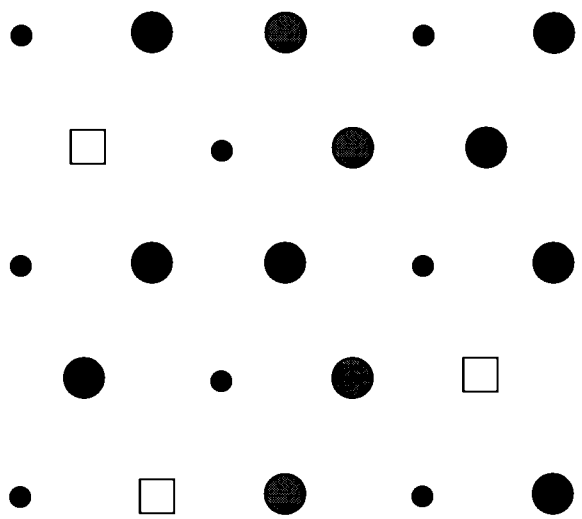

Figure 1.4: View of the Cd-P layer demonstrating random vacancies, where 1/5 of the Cd atoms have been converted to vacancies. Black circles represent P atoms, gray circles represent Cd atoms, and empty squares represent Cd vacancies.

1.3 AMP and CMP

The information in the first part of this section is primarily taken from Saenger [19], though much of it can be found in standard biochemistry textbooks.

A note on nomenclature: Nucleoside monophosphates are referred to as nucleotides, formed of a base (adenine, cytosine, guanine, uracil or thymine, abbreviated respectively by A, C, G, U or T), a ribose ring, and a phosphate group. The base + ribose combination is called a nucleoside (adenosine, cytidine, guanosine, uridine or thymidine).

The structure of the nucleotide adenosine 5′-monophosphate (AMP), also known as adenylic acid and adenosine 5′-monophosphoric acid, is depicted in Fig. 1.5 together with the numbering scheme for the atoms. H atoms are not shown in the figure, though it should be noted that there are two attached to the N6 atom, and that the O2′ and O3′ atoms are really OH groups. 5′-monophosphate refers to the bond between the phosphate and the 5′ C atom.

The structure of cytidine 5′-monophosphate (CMP), also known as cytidylic acid and cytidine 5′-monophosphoric acid, is shown in Fig. 1.6, with a similar numbering convention for the atoms as AMP. As in Fig. 1.5, H atoms are omitted in Fig. 1.6. There is a pair of H atoms connected to the N4 atom, and of course, as with AMP, the O2′ and O3′ atoms are bonded to H to form OH groups. The similarities between the two molecules are apparent from these figures, where the phosphate group and ribose ring are identical for both, while it is only in the bases adenine and cytosine that the differences appear. Adenine belongs to the purine family, formed essentially of a connected 6-member and 5-member planar ring, while cytidine is a pyrimidine, based on a single 6-member ring. AMP and CMP were chosen for this study as representatives of their families, since the other bases also belong to one or the other. Guanine is a purine, and uracil and thymine are pyrimidines.

It should be noted that in DNA, the O2′ site has just an H atom instead of OH (hence the name deoxyribonucleic acid). These deoxy-nucleotides are abbreviated by the designation dNMP. When AMP and CMP are part of a RNA or DNA molecule, the O3′ site is connected to the phosphate group belonging to the next NMP in the chain. Thus the 5′-monophosphate designation also helps to distinguish from 3′-monophosphates, where the phosphate group is bonded to the 3′ O atom, and there

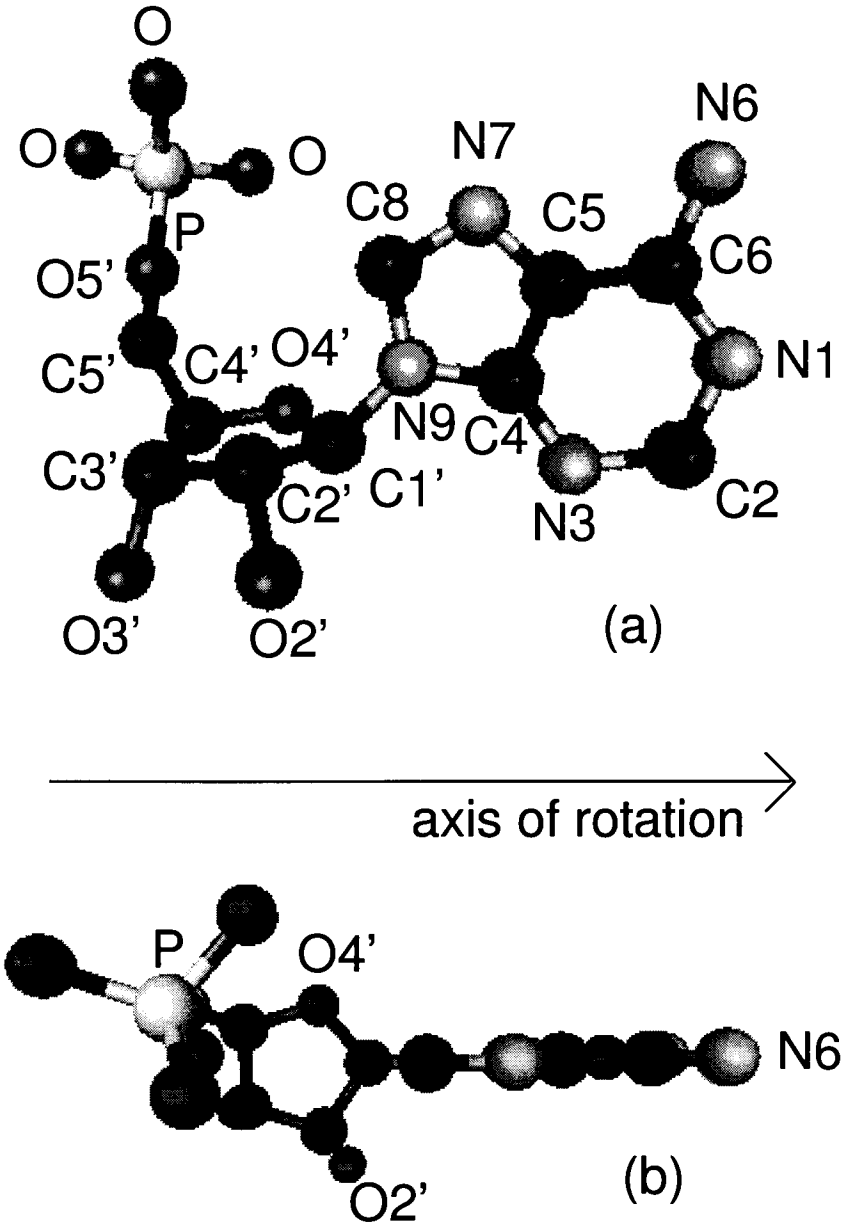

Figure 1.5: Structure of AMP: (a) shows the numbering convention for the atoms, and (b) shows the molecule rotated about the horizontal axis. H atoms are omitted.

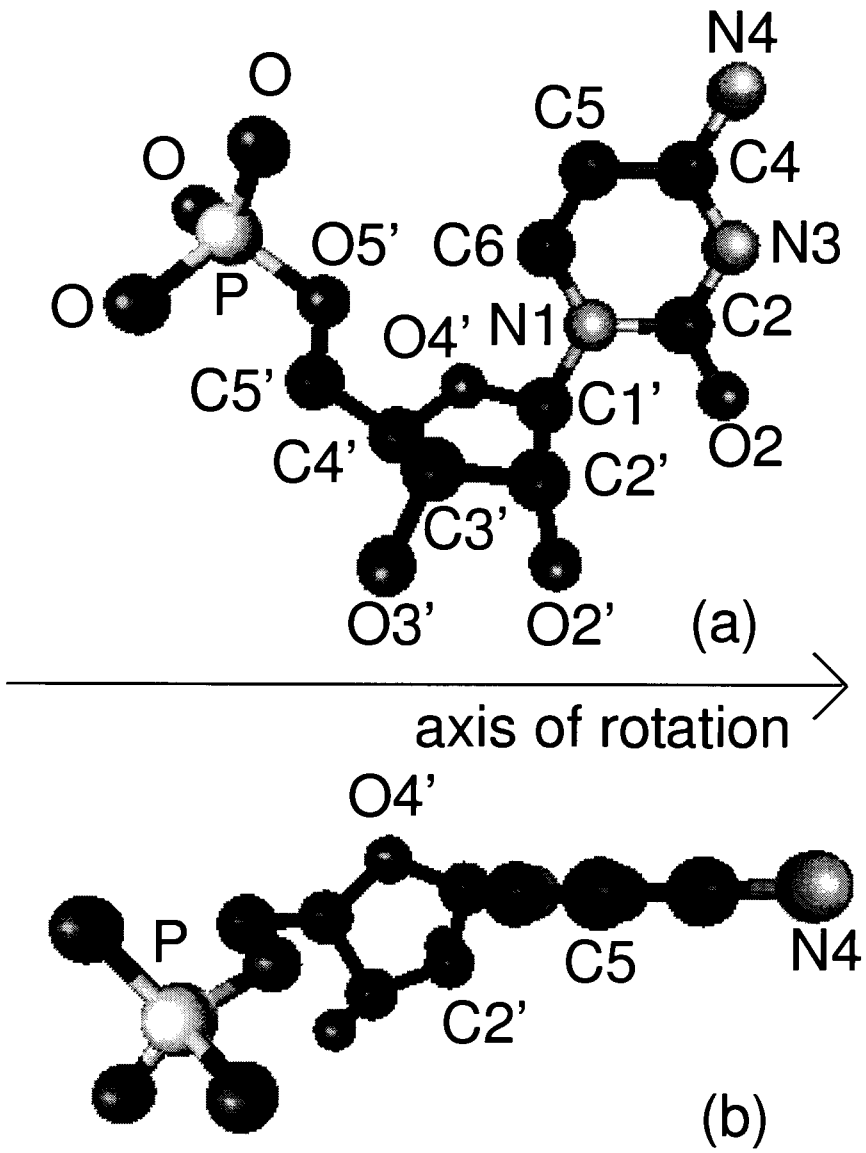

Figure 1.6: Structure of CMP: (a) shows the numbering convention for the atoms, and (b) shows the molecule rotated about the horizontal axis. H atoms are omitted.

is no phosphate in the 5′ position.

While the adenine and cytosine bases are mainly non-polar, there are sites that are capable of hydrogen bonding (in DNA and RNA, these sites form the well-known AT (or AU) and CG base pairings). For adenine, the main sites are N6, with its slightly positive H atoms, and N1, which is slightly negative. N7, which does not participate in base pairing for DNA and RNA, is also slightly negative, and is a potential site for metal coordination and other interactions. For cytosine, O2, N3 and N4 (with its H atoms) are the primary hydrogen bonding sites for base pairing.

1.3.1 Interactions with water

The interactions of AMP and CMP with water have been studied extensively over the years. One of the motivations for this is the long-known fact, mentioned by Watson and Crick as well as Franklin and Gosling in 1953 [20, 21], that the conformation of DNA depends on hydration, and that DNA can change its conformation from the well-known (post-1953) B phase to the A phase upon lowering the humidity [19].

Ganguly and Kundu [22] have presented a series of solubility measurements of the bases A, C, U and T in water and in solutions with LiCl, NaCl and KCl. Their findings show that in water and in LiCl solution, cytosine is 4-5 times more soluble, at 20 °C, than adenine. In another experimental solution study, Shih et al. [23] calculated the hydrophobicity of the bases by calculating the free energy of transfer from water to a non-polar solvent. Their results indicate that for cytosine, the free energy cost in this process is about twice as much as for adenine. Thus it is clear that cytosine has a considerably more favourable interaction with water than adenine, and since the rest of the molecules are the same, one can expect similar differences in behaviour for the full CMP and AMP molecules.

There are numerous other experimental and theoretical studies that attempt to establish which sites in DNA interact with water, and what differences appear among the various bases. For example, Schneider *et al.* [24] analysed crystallographic data from a number of previous works in order to determine the water structure around the nucleic acid bases. More recently, Shestopalova [25] performed Monte Carlo simulations to examine the dependence of nucleic acid hydration on nucleotide composition and relative humidity.

1.3.2 Acids or salts

The pH of NMP solutions is an important consideration, as it affects the ionization state of these molecules. Saenger [19] has summarized some data which show that below a pH of 6.67 for AMP and 6.62 for CMP, the phosphate changes from PO_4^{2-} to HPO_4^-. Furthermore, below a pH of 3.88 for AMP and 4.54 for CMP, one site on the base becomes protonated. For AMP, the N1 atom gains a proton, and for CMP, the N3 atom gains a proton.

Crystallization of NMPs can occur both in acid (H_2NMP) or salt form. The salt is usually formed with Na^+ (Na_2NMP), but other ions are sometimes used. X-ray diffraction of the crystals allowed the structures to be determined in detail in the 1960s [26–28]. These studies demonstrated that the H_2NMP was zwitterionic (having a positive ion and a negative ion within the same molecule), with a negatively charged phosphate group and a protonated N1 or N3 atom. In salt form, two of the phosphate oxygens form ionic bonds to the alkali metal, or to an ion with a +2 charge.

Two other studies are worth mentioning here, as they are relevant to the present work, and will be referred to in more detail again further on. The first is the work by Tajmir-Riahi and Messaoudi [29], in which the interactions of Li^+ and other alkali metal solutions with AMP are characterized by infrared and nuclear magnetic resonance (NMR) spectroscopy. The second is the recent X-ray diffraction investigation by Sugawara *et al.* [30] of a humidity-induced phase transition of crystalline Na_2CMP.

1.4 Relative humidity

Since relative humidity is mentioned frequently in this work, a brief definition is in order. The relative humidity (RH) is the ratio of water vapour pressure in the air to the saturation water pressure, at which additional water vapour condenses into liquid form. For example, at 21 °C, the saturation water vapour pressure, corresponding to 100 % RH, is 25.0 mbar, or 2.5 % of the total molar composition of air. Table 1.2 compares the values of relative humidity near room temperature to the vapour pressure of water.

Table 1.2: Conversion of relative humidity to vapour pressure of water.

Temp. (°C)	Vapour Pressure at 40 % RH (mbar)	Vapour Pressure at 80 % RH (mbar)	Saturated vapour pressure (mbar)
18	8.4	16.8	21.0
21	10.0	20.0	25.0
24	11.8	23.7	29.6

Chapter 2

Experimental procedure

2.1 Sample preparation

2.1.1 Crystal growth

Crystals of $CdPS_3$ were grown following approximately the method of Covino *et al.* [31]. A stoichiometric mixture of 0.2 mol of elemental cadmium and phosphorus powders and 0.6 mol of sulphur powder were heated in an evacuated quartz tube at 800 or 900 °C, depending on the batch, for 10 days. The different temperature did not affect the characteristics of the resulting material. The total mass of each batch was 47.91 g. The resulting material contained mostly small, mm-size crystals, but included a few large, thin single crystals about 1 - 4 cm^2 in area and 5-20 μm in thickness. The smaller crystals were ground into powder (10-50 μm size) by hand with mortar and pestle prior to ion exchange and exfoliation.

2.1.2 Ion exchange and exfoliation

Potassium ions were intercalated into the $CdPS_3$ layers, then exchanged with lithium ions, and finally exfoliated in water before being restacked in the presence of CMP or AMP.

Following the method of Lagadic *et al.* [32], 0.5 g of $CdPS_3$ powder were added to 30 mL of aqueous 2 M KCl and 6 mL 0.1 M ethylene diamine tetraacetic acid (EDTA) in 1 M $K_2CO_3/KHCO_3$ buffer at room temperature, stirring for 20 hours.

After centrifugation, the supernatant was decanted. Lagadic *et al.* have proposed that the remaining powder is described by the formula $K_{0.4}Cd_{0.8}PS_3(H_2O)_y$. In this material, Cd^{2+} ions have been removed to form vacancies, and two K^+ ions per Cd^{2+} ion have been intercalated, together with a monolayer of water, to preserve charge neutrality.

The K^+ ions are subsequently exchanged for Li^+ by adding 35 mL of a 2 M aqueous LiCl solution, and stirring for 1 hour. After centrifugation (typically at 3000 rpm) and decantation, $Li_{0.4}Cd_{0.8}PS_3(H_2O)_z$ is recovered. The stoichiometry is explored in Section 3.3. Although the ionic radius of K^+ is 1.33 Å, much larger than the 0.68 Å of Li^+, it is found [15] that K^+ intercalates more readily than Li^+ into $CdPS_3$. This may be related to the stronger coordination of Li^+ with water, as when Li^+ is intercalated, it is accompanied by a bilayer of water, while K^+ is only accompanied by a monolayer. The literature is not very clear on this point.

Upon washing 2-3 times with about 40 mL of water, the host layers separate to form a suspension of single molecular layers in water [11]. The concentration of the resulting suspension is typically around 10 mg/mL. The pH of the suspension is around 7.

The preceding steps can be summarized with the following chemical equations:

$$CdPS_3 + 0.4KCl \longrightarrow K_{0.4}Cd_{0.8}PS_3(H_2O)_y + 0.2CdCl_2 \tag{2.1}$$

$$K_{0.4}Cd_{0.8}PS_3(H_2O)_y + 0.4LiCl \longrightarrow Li_{0.4}Cd_{0.8}PS_3(H_2O)_z + 0.4KCl \tag{2.2}$$

$$Li_{0.4}Cd_{0.8}PS_3(H_2O)_z + H_2O \longrightarrow Cd_{0.8}PS_3 \text{ suspension.} \tag{2.3}$$

The single layer suspension appears milky, with some settling occurring on the order of hours. This settling takes the form of more dense suspension in the bottom third or so of the vial, but not full precipitation into powder form. Over a period of months, the system becomes less stable and begins to form byproducts such as CdS, which fall to the bottom of the vial, forming a thin yellow layer at the base.

2.1.3 Formation of restacked nanocomposites with nucleoside monophosphates

Fig. 2.1 shows a schematic depiction of the steps involved in sample preparation of the restacked nanocomposites of single layer $CdPS_3$ and nucleoside monophosphates.

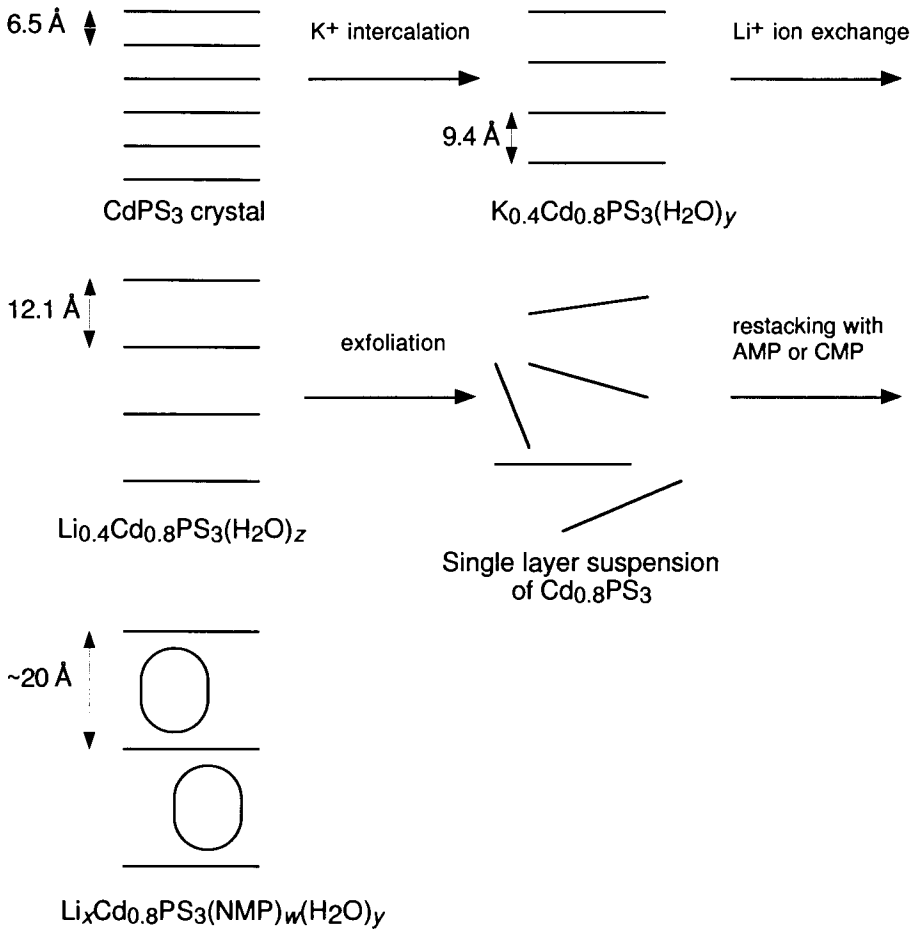

Figure 2.1: Schematic overview of sample preparation for the formation of restacked $Li_xCd_{0.8}PS_3(NMP)_w(H_2O)_y$. The lines represent the host $Cd_{0.8}PS_3$ layers. The ovals represent the NMP molecules.

CMP (Cytidine-5′-monophosphoric acid hydrate, Aldrich, 99%) or AMP (Adenosine 5′-monophosphate monohydrate, Aldrich, 99%) is dissolved in distilled water, typically at a concentration of 2 mg/mL. It was found that CMP dissolved at room

temperature, while AMP required some mild heating (around 60 °C) for several hours to aid in dissolution. The pH of these solutions was measured to be around 4.

The nucleoside monophosphate (NMP) solutions are then mixed with the $Cd_{0.8}PS_3$ suspension at a molar ratio of 1:1. The following equations describe the process (note that the value of y may be different in each case, due to different amounts of water associated with the different NMPs):

$$Cd_{0.8}PS_3 \text{ suspension} + \text{CMP} \longrightarrow Li_xCd_{0.8}PS_3(\text{CMP})_{0.3}(H_2O)_y \tag{2.4}$$

or

$$Cd_{0.8}PS_3 \text{ suspension} + \text{AMP} \longrightarrow Li_xCd_{0.8}PS_3(\text{AMP})_{0.5}(H_2O)_y. \tag{2.5}$$

Determination of the relative concentrations of AMP or CMP, as well as other compositions mentioned above, is discussed in Chapter 3.

The pH of the combination is typically 4 - 4.5. No visible flocculation occurs upon addition of an NMP solution to the $Cd_{0.8}PS_3$ suspension over the same period as for the $Cd_{0.8}PS_3$ suspension alone (i.e. months). The films of these materials can be made as follows. The suspension containing NMP is stirred briefly, and then dropped on a glass slide and left to dry in air at room temperature. The films thus obtained tend to be 500 - 1000 Å thick.

2.2 Characterization Techniques

2.2.1 EDS

Energy dispersive X-ray spectra were taken on an FEI Dualbeam Strata 235 with EDAX X-ray analyzer to determine the stoichiometry of the samples. The results are presented in Chapter 3.

2.2.2 XRD

Two X-ray diffractometers were used for this thesis: a Philips model PW 1730 and a Siemens D5000 Diffractometer. In both cases, experiments were conducted using Cu K_α radiation ($\lambda = 1.542$ Å).

2.2.3 Humidity control apparatus

In order to determine the effect of humidity on the structure of the $CdPS_3$/NMP composites, it was necessary to vary the humidity in the sample chamber of the X-ray diffractometer. Therefore a humidity control apparatus, depicted in Fig. 2.2, was assembled.

The sample chamber was maintained at a given humidity by passing controllable flows of nitrogen gas in parallel through a dry and a wet chamber, assigning the proportions of wet and dry air to get the desired relative humidity in the chamber. The wet chamber, an aluminum box measuring about 8 cm × 0.5 cm × 2 cm, contained liquid water at the bottom, and as dry air entered, it would pass over the water and become humid. A water bubbling column was placed at the exit of the wet chamber to aid in humidifying the wet flow.

Flow control was achieved with a pair of MKS model 1159B mass flow controllers (MFCs). In these controllers, the amount of gas allowed to flow through the exit valve is proportional to a DC voltage input. The MFCs maintain a known flow by measuring a small portion of the incoming gas in a laminar flow through a path parallel to that of the bulk of the incoming gas. The temperature profile is determined, and feedback circuits ensure that the temperature profile corresponds to the desired flow rate. For the experiments done in this thesis, a 4 V input voltage was used, corresponding to a flow rate of 160 sccm (standard cubic centimeters / minute). A variable resistor in a voltage divider-like circuit was used to assign different portions of the 4 V to the wet or dry flow, as desired.

An Omega RH411 digital thermo-hygrometer was placed near the sample chamber to record temperature and relative humidity. Air from the sample chamber flowed past the probe. For this set-up, "all-dry" flow corresponded to 1-2 % RH, while "all-wet" flow gave 82 %. All measurements were taken at room temperature, usually 20-22 °C.

A large change in humidity, e.g. drying out the sample chamber from a RH of 50 % to a final RH of 2 %, took on the order of 1-2 hours to achieve stability of within 1 % RH. Over longer periods of time, and in particular when the room temperature changed, it was found that the RH could drift by as much as 10 %. Even if the sample chamber temperature was maintained, an increase in the lab temperature could cause greater evaporation of water in the water chamber, and therefore increase the RH of

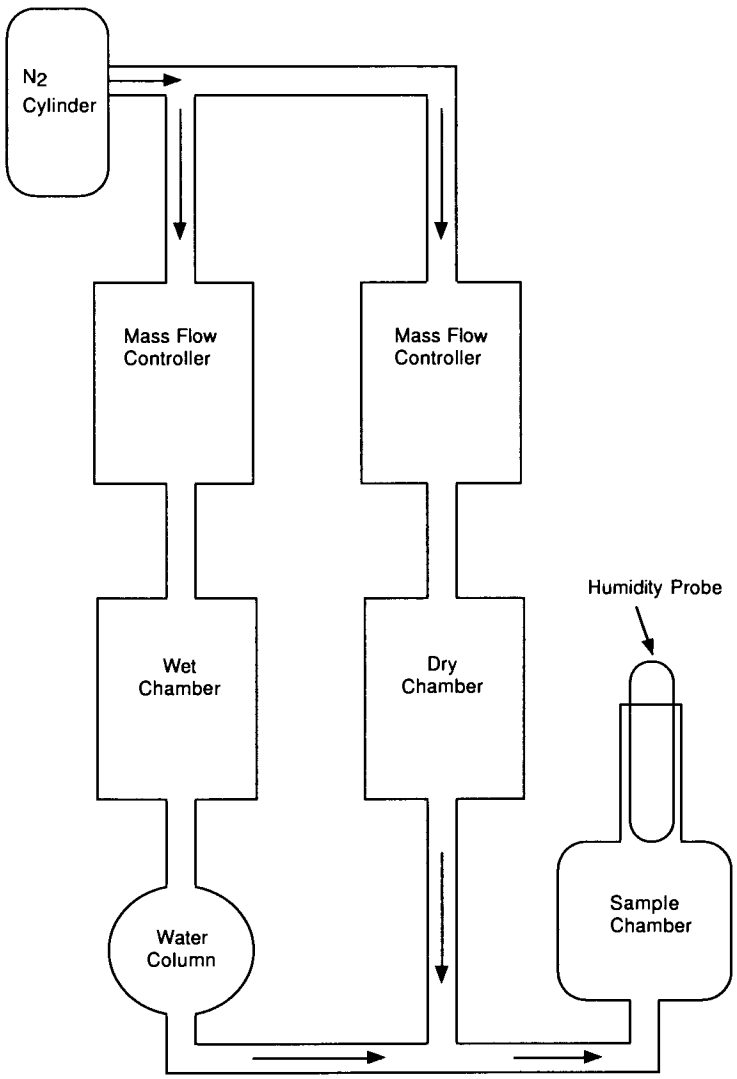

Figure 2.2: Block diagram of humidity control apparatus for samples in X-ray diffraction chamber.

the sample chamber. Similarly, a reduction in lab temperature could cause a reduction in sample chamber RH. Since a typical X-ray diffraction run took about 20 minutes for the humidity experiments, the variation in humidity was minimal on that timescale.

Chapter 3

Determination of sample composition by energy dispersive spectroscopy

In order to determine the composition of our samples, we used energy dispersive spectroscopy (EDS). In this experiment, electrons from a scanning electron microscope excite the atoms in the sample. The excited electrons then emit X-rays characteristic of the atoms as they relax back to the ground state. The emitted X-rays are then measured by a lithium-drifted silicon diode detector, in which the number of electron-hole pairs created by the absorption of an X-ray is proportional to the energy of that X-ray.

We obtained compositional information on samples of crystalline $CdPS_3$, on K^+-intercalated $CdPS_3$, on restacked suspensions with no guest molecule other than Li^+ and H_2O, and on the restacked suspensions with AMP and CMP included. All scans used a 10 kV electron beam, with a current of 400 μA.

The data were analyzed by a built-in computer program called EDAX which calculated and displayed the atomic percents of each element. This program is designed to correct for some of the factors that can modify the relation between compositional ratios and actual ratios of emitted X-rays.

While in some cases this analysis is successful, with a large number of elements in the sample, it is worth keeping in mind that some of the effects will not be adequately

compensated for, and some data may be somewhat unreliable. Some of these effects that are addressed by the software are outlined in Chapter 10 of Reimer as follows [33]:

1. The maximum path length of electron trajectories (so-called Bethe length) depends on the sample composition. This path length affects the probability of ionization, and thus the emission of characteristic X-rays from the sample.

2. A certain fraction of electrons are backscattered, and those that are at energies larger than the ionization energy of a given element will fail to cause the emission of X-rays from that element in the sample. This failure produces a reduction in the emission of X-rays from the given element.

3. X-rays can be absorbed inside the sample.

4. X-ray fluorescence can occur, where the emission of X-rays from one element in the sample can ionize another element in the sample, causing increased emission from the latter element.

3.1 EDS measurements on crystalline $CdPS_3$

$CdPS_3$ powder was placed on a piece of two-sided sticky carbon tape, the other side of which adhered to the aluminum sample holder. The EDAX analysis software gave a composition of $Cd_{1.03}PS_{2.72}$, averaging over data taken in four different regions of the sample. The area of these regions was typically in the range of 100 μm^2 - 1000 μm^2.

A typical X-ray emission spectrum is shown in Fig. 3.1. This spectrum corresponds to "region 1" of the sample. As with most of the samples measured, the number of counts corresponding to peaks in the spectrum is in the 100-1000 range.

The data for all four regions of the sample are given in Table 3.1 in order to give an idea of the range of compositions found in a typical sample. This range is similar to that found in the other samples described in subsequent sections below.

Since the composition of the sample as a whole had significantly less S than we had expected, we then analyzed a sample of CdS crystal as a reference. The reason for the lower than expected intensity of S is likely due to the aforementioned possibility that the analysis software does not compensate correctly for the factors listed above. This sample was also mounted on a carbon tape - covered aluminum sample holder. The

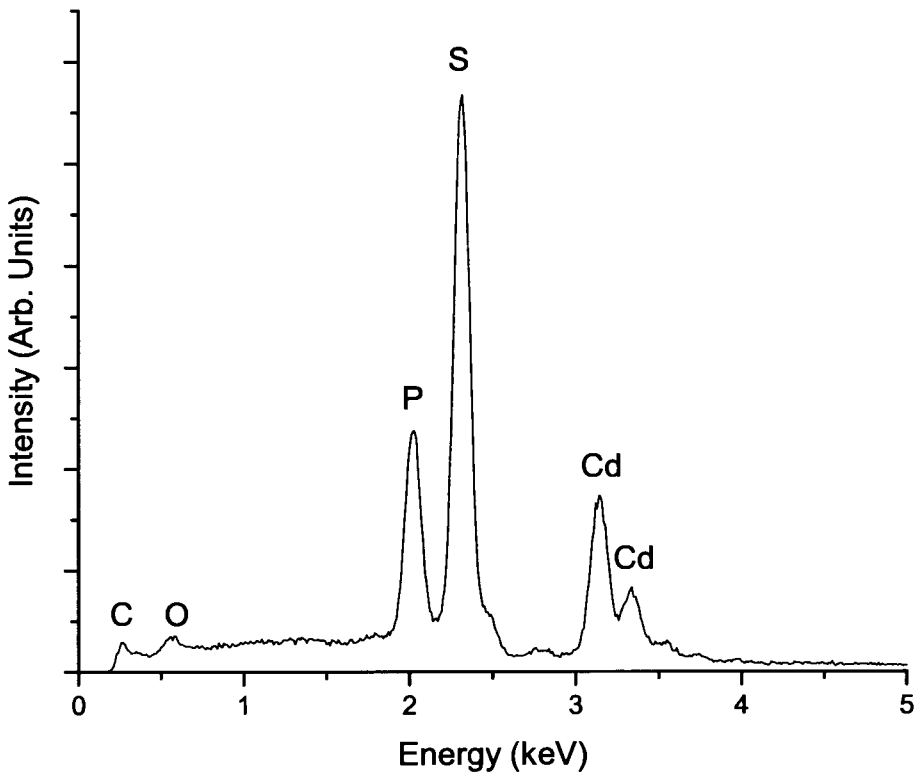

Figure 3.1: X-ray emission spectrum for crystalline $CdPS_3$. Beam voltage is 10 kV.

composition of this sample was given as $CdS_{0.88}$. Thus in both samples, the amount of S was underestimated by around 10% relative to that of Cd. In order to make up for this apparent under-counting of S, 10% was added to the calculated atomic percent of S in some of the other samples, as mentioned in the next sections.

As shown in Table 3.1, region 3 has a high proportion of O and a lower S value than the other regions. This may be due to some degree to partial oxidation, where O has taken the place of S in the sample.

A second sample of crystalline $CdPS_3$ was also analyzed over three different regions. This sample, which came from a different batch of $CdPS_3$ grown at a different time, gave an average composition value of $Cd_{0.97}PS_{2.73}$, in good agreement with the batch discussed above.

Table 3.1: Compositions of different regions of a crystalline $CdPS_3$ powder sample.

Region of Sample	Composition including C, O	Composition without C, O
1	$C_{1.07}O_{0.28}Cd_{1.04}PS_{2.86}$	$Cd_{1.04}PS_{2.86}$
2	$C_{1.43}O_{0.27}Cd_{1.07}PS_{2.87}$	$Cd_{1.07}PS_{2.87}$
3	$C_{1.27}O_{0.96}Cd_{0.92}PS_{2.38}$	$Cd_{0.92}PS_{2.38}$
4	$C_{0.94}O_{0.55}Cd_{1.09}PS_{2.78}$	$Cd_{1.09}PS_{2.78}$
Average	$C_{1.17}O_{0.53}Cd_{0.1.03}PS_{2.72}$	$Cd_{1.03}PS_{2.72}$

It should be noted that there is a background of emissions from C and O atoms in most of the samples analyzed (see Table 3.1), whether on tape or directly placed on the aluminum substrate. The signal from C is much stronger for the samples on the carbon tape. Part of this background may be due to contamination of the sample or substrate surfaces, and exacerbated by the charging of the samples [33], all of which are electrically insulating.

3.2 EDS measurements on $KCdPS_3$ powder

A sample of K^+-intercalated $CdPS_3$ was dried, and some of the dry powder was placed on a carbon tape - covered Al sample holder. Averaging over three regions of the sample, and adding 10% to the S value, the following composition formula was obtained: $K_{0.40}Cd_{0.76}PS_{3.05}$. This formula is quite consistent with those of other groups working with the same compound, as shown in Table 3.2. Results for the restacked single layer suspension are also shown in the table. Lithium can not be detected with this instrument, and H_2O was ignored since most of it is expected to be removed under vacuum.

3.3 EDS measurements on restacked single layer film

A drop of the single layer suspension of $CdPS_3$ was applied directly on to the aluminum sample holder and allowed to dry in air. Based on X-ray diffraction results (see Section

Table 3.2: A selection of compositions of $CdPS_3$ after intercalation with K^+ (10 % correction applied) or K^+ followed by Li^+ (10 % correction not applied).

Reference	Composition
[15]	$Cd_{0.75}PS_3K_{0.5}(H_2O)_{1.0}$
[34]	$Cd_{0.742}PS_3K_{0.57}(H_2O)_{1.2}$
[17]	$Cd_{0.77}PS_3K_{0.45}(H_2O)$
Present Work	$Cd_{0.76}PS_{3.05}K_{0.40}(H_2O)_y$
[32]	$Cd_{0.84}PS_3Li_{0.35}(H_2O)_2$
Present Work	$Cd_{0.85}PS_{2.91}Li_x(H_2O)_y$

4.1), upon drying, the suspension restacks with a bilayer of water between the host $CdPS_3$ layers. The raw composition obtained was $Cd_{0.85}PS_{2.91}$, averaging over three regions of the sample. There was no evidence of any remaining K.

The 10% underestimation of sulphur that was observed for the crystal samples may not be valid for the case of the restacked sample. If we do take the 10% underestimate of sulphur into account, we get a composition of $Cd_{0.85}PS_{3.2}$. However, without adding the additional 10% for sulphur, our results agree relatively well with those of Lagadic *et al.* [32], who used chemical elemental analysis in their work. This comparison is shown in Table 3.2. It appears that there is some loss of P in the Li-intercalated compounds, as both our results and those of Lagadic *et al.* have a higher Cd/P atomic ratio than in the K-intercalated compounds, as can be seen in the table. This loss of P is likely caused by the formation of phosphate ions in solution due to attack from oxygen.

3.4 EDS measurements on restacked composites with AMP or CMP included

As with the restacked single layer suspension, a drop of the mixed suspension of $CdPS_3$ single layers and NMP solution was placed directly on the aluminum substrate and left to dry in air.

A typical spectrum for the restacked sample with AMP is shown in Fig. 3.2.

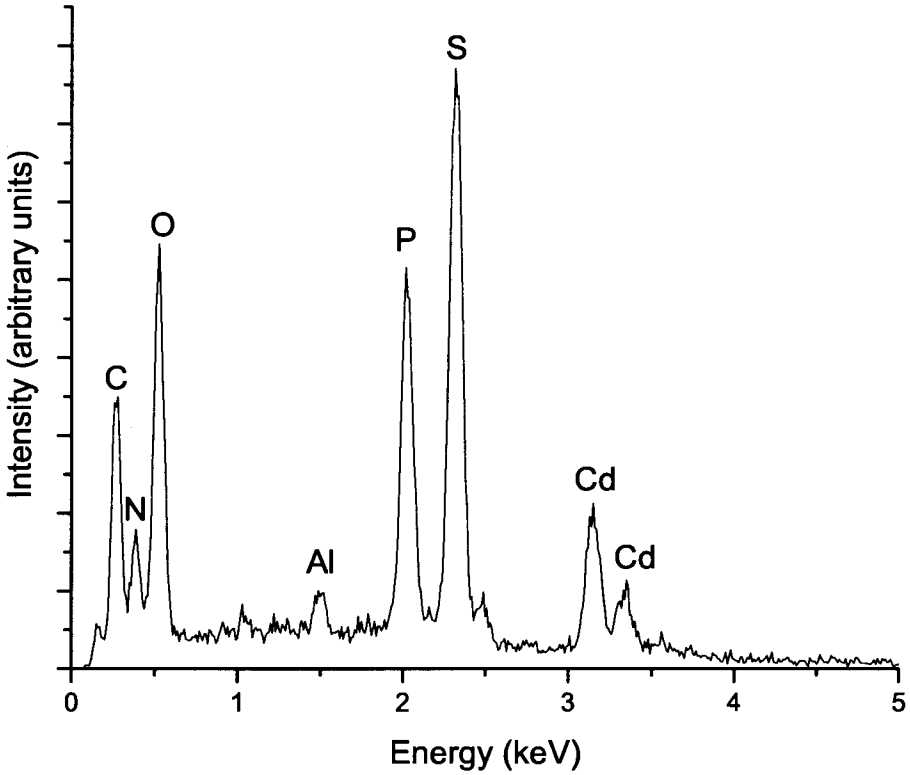

Figure 3.2: X-ray emission spectrum for a restacked $CdPS_3$/AMP sample. Beam voltage is 10 kV.

Calculations of the composition of these samples is made more complicated by the fact that phosphorus is present in both the host and guest material. This fact may cause errors in the composition data obtained. However, due to the similarity of the composite to the restacked single layer samples, both of which were deposited directly on the aluminum substrate, and both of which were dropped from suspension and dried, we can use the composition of the restacked single layer sample as a reference. Conversely, we can make use of the fact that P is in both host and guest to calculate the composition, assuming a known host composition and using the remainder of P to calculate the ratio of guest / host.

It should be noted that the Cd:S ratio in both the restacked samples with AMP and CMP comes out to 0.31, compared to the 0.29 found for the restacked single layers with no guest molecule. These results are sufficiently close to justify using the final

entry in Table 3.2 to calculate the P content in the host layers when AMP or CMP are present. For the case of host layers + guest, we assume that we have $Cd_{0.85}P$ or that we have $PS_{2.91}$, as with the restacked single-layer samples, but not both.

3.4.1 CMP

For the CMP sample, a region was found that contained no Cd or S, but that did contain C, O, N and P. It was assumed that this was a region of excess CMP that was not included between the host $CdPS_3$ layers. EDS analysis of this region allowed for a calibration of the guest molecule. Each molecule of CMP contains the following atoms (excluding hydrogen): 9 C, 8 O, 3 N and 1 P, so the ideal composition in this region would be $C_9O_8N_3P$.

The composition found in this region was $C_{12.2}O_{7.5}N_{3.0}P_{1.0}$, normalized to a value of N=3.0. The O and P values fit well, but the C value was about 36% too high. This is consistent with the fact that there was a background of C observed in all of our samples, as mentioned above.

The compositional information of the inclusion compound was obtained over two other regions of the sample. There are several ways to approach this calculation. First, assuming that $Cd_{0.85}P$ is correct for the host layers, and that the as-given S value is correct, the remainder of the P gives the CMP ratio. Using this method, we get a composition of $Cd_{0.85}PS_{2.77}(CMP)_{0.22}$. If, instead, we assume that $PS_{2.91}$ is the correct ratio, i.e. normalizing to the given S value, we get a composition of $Cd_{0.89}PS_{2.91}(CMP)_{0.29}$. A third method is to assume that the atomic percent of N is three times that of P in CMP, as was found to be true in the region of CMP alone. With this method, the remainder of the P is contained in the host layer. Using this approach, we obtain a composition of $Cd_{0.93}PS_{3.03}(CMP)_{0.34}$. It should be noted that the C (corrected by 36%), N and O values are consistent with the region of CMP alone described above, even in this region of host/guest compound. However, the amount of P does not seem to be consistent with our assumptions about the host composition as well as with the composition of CMP. At the same time, samples with a large number of elements are particularly susceptible to errors in EDS analysis, due to all of the possible interactions and effects described in the introduction to EDS above. In order to get around this difficulty, a final approach to this calculation is to

assume that we have $Cd_{0.85}P$, that the atomic percent value of N is correct, and to combine these without using P in the calculation. With this method, we arrive at a composition of $Cd_{0.85}PS_{2.77}(CMP)_{0.31}$. The composition $Cd_{0.85}PS_{2.7}(CMP)_{0.3}$ is used in the rest of the thesis to refer to these samples.

Table 3.3 shows a summary of these calculations, and which assumptions are used for each calculation, for the $CdPS_3$/CMP samples.

Table 3.3: Compositions calculated for $CdPS_3$/CMP and $CdPS_3$/AMP samples.

Elements used for Calculation	Composition
$Cd_{0.85}$, P (host)	$Cd_{0.85}PS_{2.77}(CMP)_{0.22}$
P, $S_{2.91}$(*host*)	$Cd_{0.89}PS_{2.91}(CMP)_{0.29}$
N_3, P (CMP)	$Cd_{0.93}PS_{3.03}(CMP)_{0.34}$
$Cd_{0.85}$ (host), N_3 (CMP)	$Cd_{0.85}PS_{2.77}(CMP)_{0.31}$
$Cd_{0.85}$, P (host)	$Cd_{0.85}PS_{2.72}(AMP)_{0.39}$
P, $S_{2.91}$ (host)	$Cd_{0.91}PS_{2.91}(AMP)_{0.48}$
N_5, P (AMP)	$Cd_{0.99}PS_{3.17}(AMP)_{0.61}$
$Cd_{0.85}$ (host), N_5 (AMP)	$Cd_{0.85}PS_{2.72}(AMP)_{0.53}$

3.4.2 AMP

The ideal composition of AMP, excluding hydrogen, is $C_{10}O_7N_5P$. For the restacked AMP inclusion compound, we follow the same four methods of calculation as outlined above for $CdPS_3$/CMP. If we first assume that we have $Cd_{0.85}P$ in the host layers, then we get a composition of $Cd_{0.85}PS_{2.72}(AMP)_{0.39}$. If we start instead from the assumption that we have $PS_{2.91}$ in the host layers, then we obtain a composition of $Cd_{0.91}PS_{2.91}(AMP)_{0.48}$. Thirdly, if we take the given atomic percent of N to be 5 units, and use the remaining P to calculate the host layer composition, we obtain a formula of $Cd_{0.99}PS_{3.17}(AMP)_{0.61}$. Using the fourth approach, with $Cd_{0.85}$ and N_5 as the standards, we obtain a composition of $Cd_{0.85}PS_{2.72}(AMP)_{0.53}$. Table 3.3 shows a summary of these calculations, and which assumptions are used for each calculation, for the $CdPS_3$/AMP samples. The composition $Cd_{0.85}PS_{2.7}(AMP)_{0.5}$ is used in the rest of the thesis to refer to these samples.

Chapter 4

X-ray diffraction patterns of starting materials

In this chapter, a series of XRD patterns will be presented for the $CdPS_3$ materials that are obtained in the steps leading to exfoliation, and for the as-received AMP and CMP powders. The number of counts for the strongest peaks varies, but is typically found in the range of 10^3 - 10^5, which also applies to all patterns in the rest of the thesis.

4.1 XRD patterns of $CdPS_3$, $K_{0.4}Cd_{0.76}PS_3(H_2O)_y$ and $Li_xCd_{0.85}PS_3(H_2O)_y$

The X-ray diffraction pattern for crystalline $CdPS_3$ is shown in Fig. 4.1. The (001) peak is quite dominant, showing that the powder is somewhat oriented, with the basal planes more likely to be parallel to the substrate. The other peaks are indexed according to the monoclinic structure with the parameters given in the Introduction.

The pattern for $K_{0.4}Cd_{0.76}PS_3(H_2O)_y$, with only the (001) and (002) peaks, is displayed in Fig. 4.2. The (001) peak gives a layer spacing of 9.42 Å, corresponding to a monolayer of water increase over the 6.55 Å spacing of the (001) peak in the original crystal, where the nominal size of a water molecule is taken to be 2.8 Å. It should be noted that the spacing reported in the literature varies slightly for this compound, apparently depending on temperature and relative humidity. The spacings reported

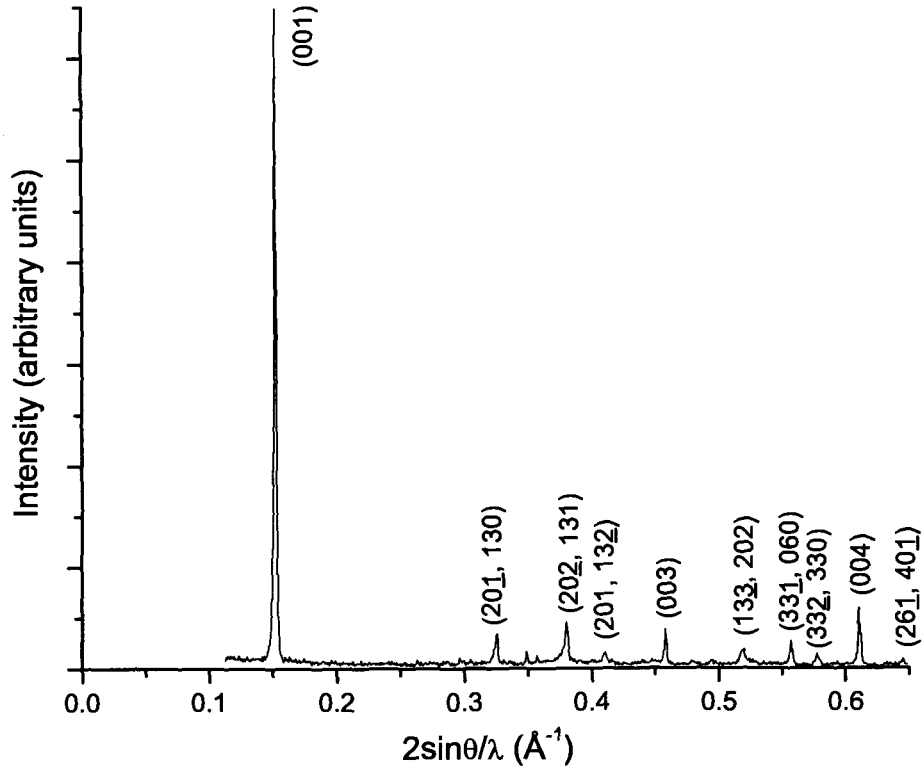

Figure 4.1: XRD pattern of crystalline $CdPS_3$.

are presented in Table 4.1. It should also be pointed out that this compound is still crystalline with the monoclinic structure of the original crystal, with changes to the c-axis spacing and the angle β as a result of the interlayer expansion [15, 34].

After the K^+-intercalated compound is ion-exchanged for Li^+, the diffraction pattern changes again, to give a bilayer of water increase over the initial crystal layer spacing. The XRD pattern is shown in Fig. 4.3. The (001) peak corresponds to a spacing of 12.4 Å.

The disappearance of the $K_{0.4}Cd_{0.76}PS_3(H_2O)_y$ (001) peak and its replacement by a new peak make it easy to tell when the ion exchange has been completed. Similarly, the earlier disappearance of the original (001) peak for the crystal, to be replaced by the (001) peak for the K^+-intercalated material, allows for a convenient monitoring of the K^+ intercalation.

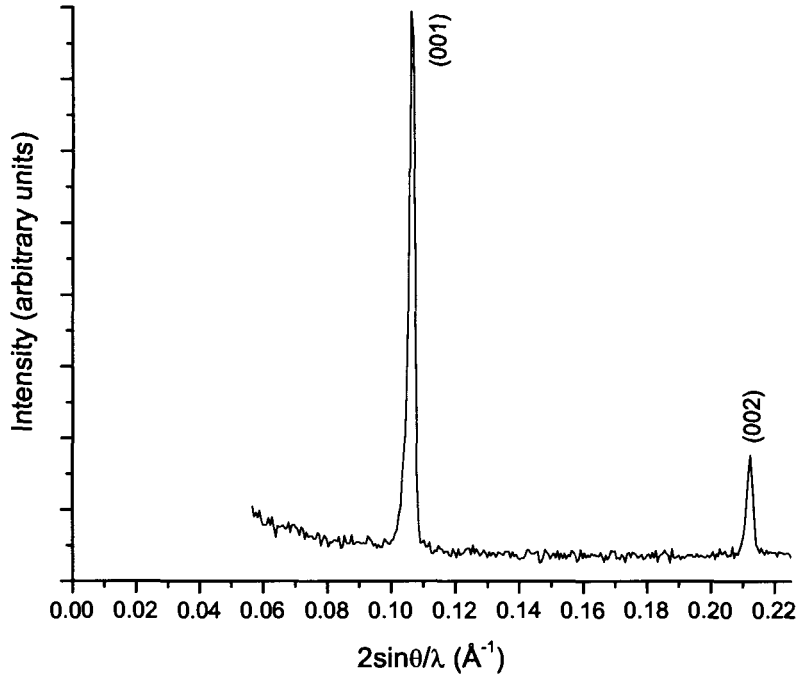

Figure 4.2: XRD pattern of oriented $K_{0.4}Cd_{0.76}PS_3(H_2O)_y$ at room temperature and 40 % RH.

4.2 XRD patterns of AMP and CMP

X-ray diffraction patterns of the as-received crystal powders of AMP and CMP were taken, and are shown in Figs. 4.4 and 4.5.

These patterns were a useful reference to help identify recrystallization of excess NMPs in certain samples of the hybrid inclusion compounds [8]. The XRD patterns shown in this thesis for $Cd_{0.85}PS_{2.7}(AMP)_{0.5}$ and $Cd_{0.85}PS_{2.7}(CMP)_{0.3}$ do not have any peaks associated with crystalline AMP or CMP.

Table 4.1: Reported basal plane spacings of $K_{0.5}Cd_{0.75}PS_3(H_2O)_y$.

Reference	Spacing (Å)	Comment
[15]	9.20	
[34]	9.522	
[35]	9.45	in air
[35]	9.25	vacuum
Present Work	9.42	40 % RH

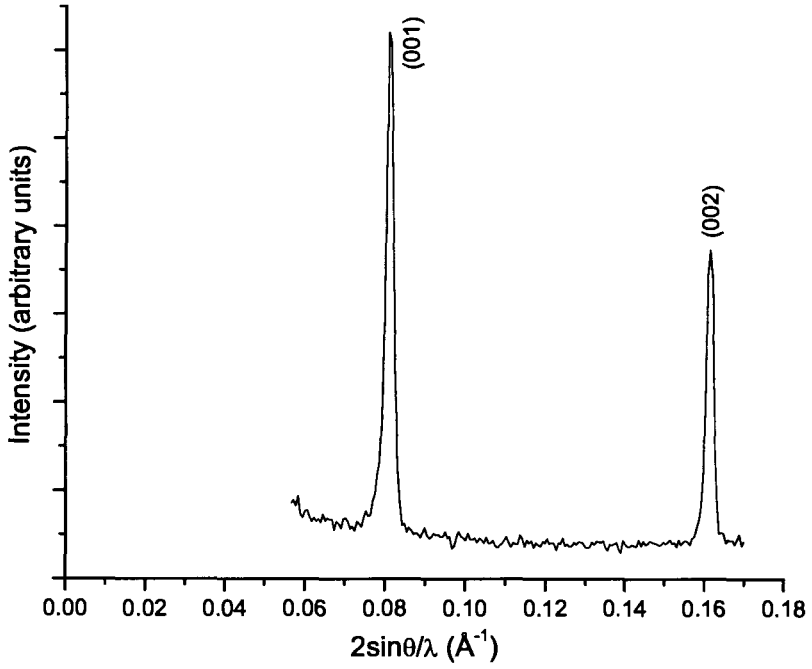

Figure 4.3: XRD pattern of oriented $Li_xCd_{0.85}PS_3(H_2O)_y$ at room temperature and 40 % RH.

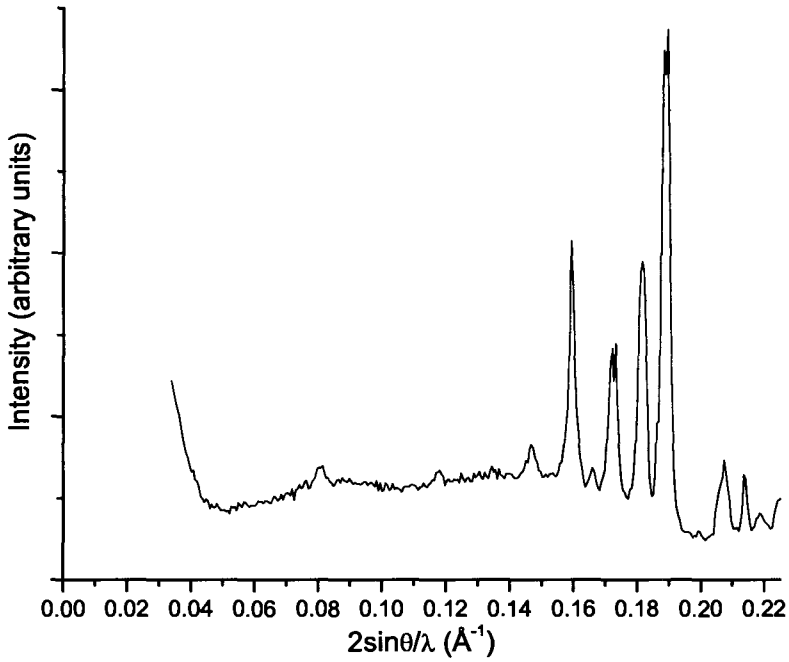

Figure 4.4: XRD pattern of AMP at 56 % RH.

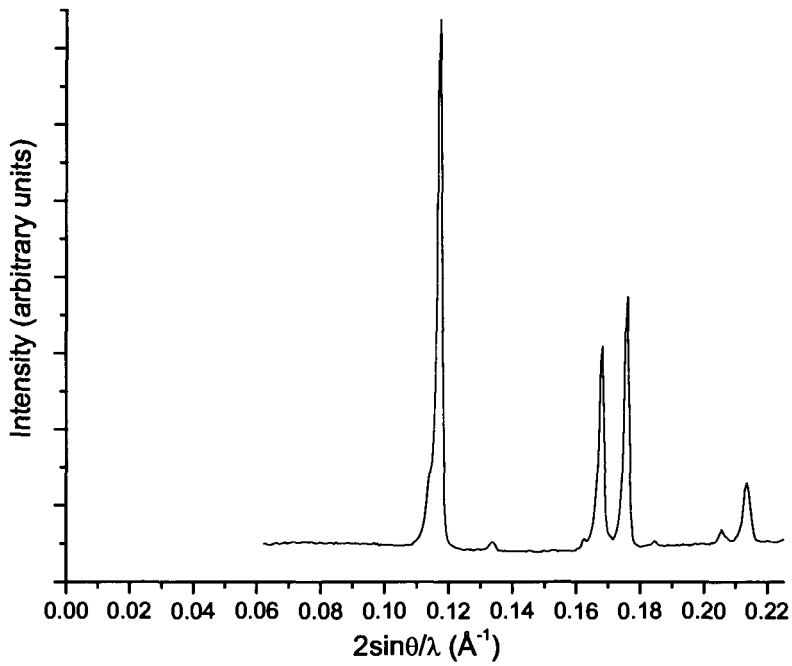

Figure 4.5: XRD pattern of CMP at 27 % RH.

Chapter 5

X-Ray diffraction studies of $Cd_{0.85}PS_{2.7}(AMP)_{0.5}$

5.1 XRD Pattern of $Cd_{0.85}PS_{2.7}(AMP)_{0.5}$

X-ray diffraction can provide a great deal of information about the structure of the $Cd_{0.85}PS_{2.7}(AMP)_{0.5}$ films. The X-ray diffraction pattern of an oriented film of $Cd_{0.85}PS_{2.7}(AMP)_{0.5}$ is shown in Fig. 5.1. The host layer planes are oriented parallel to the glass substrate. Fourteen $00l$ peaks are observed in this pattern, corresponding to a host basal plane spacing of 19.6 Å. The four negative intensity spikes in the region between 0.35 and 0.4 $Å^{-1}$ are clearly instrumental glitches, and will be ignored in all further discussion and analysis of this data set. The fact that there are fourteen peaks, all corresponding to the same spacing, allows for further analysis of this pattern.

The first type of analysis concerns electron density calculations, where the electron density of the unit cell is extracted from the XRD pattern. Thus we can glean some information regarding the arrangement of atoms in the unit cell by this method. In the XRD pattern of Fig. 5.1, it is clear that the (005) and (007) peaks are very weak, while the (006) peak is quite strong. This type of variation is largely due to the structure factor, which is closely related to the electron density. Electron density calculations attempting to explain these and other features of Fig. 5.1 will be seen in more detail following a brief discussion of the effect of humidity on the XRD pattern.

The second type of analysis concerns the peak widths. At higher orders, the peak

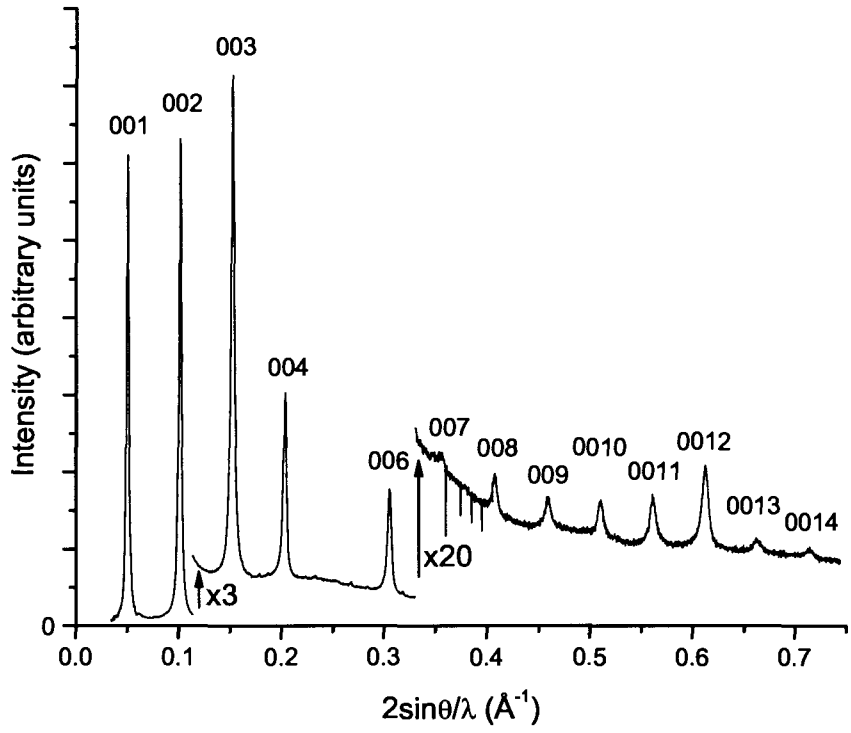

Figure 5.1: X-ray diffraction pattern for an oriented film of $Cd_{0.85}PS_{2.7}(AMP)_{0.5}$ at 29 % RH.

widths broaden appreciably, and the amount of broadening is related to the disorder of the system. We will examine this in more depth following the discussion of electron density.

5.1.1 Humidity

The diffraction pattern in Fig. 5.1 was taken at room temperature, at a relative humidity of 29 %. It should be noted at this point that for a wide range of humidities, the diffraction pattern of $Cd_{0.85}PS_{2.7}(AMP)_{0.5}$ does not change significantly, and the spacing varies by no more than about 0.5 Å between 0 % RH and around 80 % RH at room temperature. Above 80 %, the layer expansion begins to increase rapidly. This

behaviour will be compared to that of the restacked system with CMP included in the Conclusions chapter.

5.2 Electron density calculation

In order to learn something about the arrangement of the guest molecules, one can calculate the electron density along the direction normal to the restacked host planes from the X-ray diffraction pattern.

The integrated intensity of a peak (found by calculating the area under the curve) is given by the following expression [36]:

$$I \propto |F|^2 \left(\frac{1+\cos^2 2\alpha \cos^2 2\theta}{\sin 2\theta}\right) e^{-2M}. \tag{5.1}$$

F is the structure factor, which is related to the types of atom in the unit cell and their positions in the unit cell.

2α is the diffraction angle of the graphite monochromator ($= 26.3°$), and 2θ is the diffraction angle of the peak in question. The $1+\cos^2 2\alpha \cos^2 2\theta$ term is the polarization factor for the X-ray beam scattering off both the sample and the monochromator.

The $1/\sin 2\theta$ term is the Lorentz factor, which takes into account the geometry of the diffractometer set-up for single crystal or oriented film samples (for powder samples it needs to be modified).

The last term, e^{-2M}, is called the Debye-Waller factor, or temperature factor. This term accounts for the effect of thermal vibrations on peak intensity. The Debye-Waller factor tends to dampen out the intensity of higher-order peaks. In particular, M can be written as:

$$M = 8\pi^2 \bar{u^2} \left(\frac{\sin\theta}{\lambda}\right)^2 = B\left(\frac{\sin\theta}{\lambda}\right)^2. \tag{5.2}$$

Here, λ is the wavelength of the X-ray radiation, or 1.54 Å for our Cu K_α X-rays. $\bar{u^2}$ is the mean square displacement, in the perpendicular direction, of the atomic planes due to vibration. $\sqrt{\bar{u^2}}$ is typically on the order of tenths of Ångstroms, corresponding to B on the order of 1 - 10 Å^2. Specifically, for $B = 5$, $\sqrt{\bar{u^2}} = 0.25$Å, while for $B = 10$, $\sqrt{\bar{u^2}} = 0.35$Å. For inorganic crystals, B is typically in the range 2.5 - 3.5 Å^2, while for organic solids it can be around 10 Å^2 or more.

For one-dimensional systems like our oriented films, the electron density along the direction perpendicular to the planes is related to the structure factor by the following equation:

$$\rho(z) = C + D\sum F_{00l}\cos(2\pi lz), \tag{5.3}$$

where C and D are constants, and F_{00l} is the structure factor of a given $00l$ peak.

F_{00l} can be extracted from the intensity by inverting equation 5.1. This gives the following equation for structure factor in terms of the intensity I_{00l} of the lth order peak:

$$F_{00l} \propto \sqrt{\frac{I_{00l}e^{2M}}{LP}}, \tag{5.4}$$

where L is the Lorentz factor and P is the polarization factor, as described above, and M is given by equation 5.2.

The values for F_{00l} are real for a symmetric unit cell, which we will assume for our samples. The host layers are symmetric about the plane of the Cd atoms, and the guest molecules would be expected to arrange themselves in a way that is symmetric on average as well.

The values of F_{00l} can also be positive or negative. For a heavy atom system, where one type of atom dominates the scattering, all F_{00l} are positive. However, in our case there will be some F_{00l} which we expect to be negative, due to interference between, for example, the sulfur atoms (3 S atoms have 48 electrons) and the cadmium atoms (0.85 Cd atom has 41 electrons). Determination of which F_{00l} are positive and which are negative will be discussed more specifically below.

5.2.1 Calculation of electron density for an oriented film of $Cd_{0.85}PS_{2.7}(AMP)_{0.5}$

The diffraction pattern of Fig. 5.1 shows 14 $00l$ peaks. Following the steps outlined above, we can attempt to calculate the structure factors of each peak, and hence the electron density. However, in order to find out the signs of the individual structure factors, some modelling and calculation of structure factors is required. The absolute values calculated from the data for B = 0 Å^2, B = 5 Å^2 and B = 10 Å^2 are shown in

Table 5.1. As noted above, for this system a value betweeen 5 Å^2 and 10 Å^2 would be expected for B, and for most of the rest of this section, comparisons will be made to the experimentally derived F for B = 5 Å^2.

Table 5.1: Structure factor values derived from experiment and calculated for B = 0 Å^2, B = 5 Å^2 and B = 10 Å^2.

Order of Peak	Angle 2θ (degrees)	Intensity (arbitrary units)	Lorentz - Polarization Factor	Structure Factor B = 0 Å^2	B = 5 Å^2	F B = 10 Å^2
1	4.51	14100	12.682	129	129	130
2	9.02	12600	6.309	173	175	177
3	13.55	5830	4.164	145	149	154
4	18.15	2220	3.071	104	110	116
5	22.55	31	2.437	13.9	15.1	16.4
6	27.3	1450	1.976	105	118	133
7	31.86	31	1.659	16.7	19.5	23
8	36.68	73.5	1.408	28.0	34.5	42.4
9	41.52	81.8	1.213	31.8	41.4	53.9
10	46.38	100	1.059	37.7	52.3	72.4
11	51.32	154	0.9331	49.8	73.9	110
12	56.38	288	0.8298	72.2	115	184
13	61.52	52	0.7460	32	56	98
14	66.88	39	0.6775	29	56	105

The theoretical structure factor can be calculated using the known values of atomic form factors and positions of the atoms in the unit cell. The structure factor F is given by the following equation:

$$F_{00l} = \int_{unit\ cell} \rho(z) e^{2\pi i l z} dz. \tag{5.5}$$

The electron density within the unit cell, $\rho(z)$, is found by adding the contributions of the atomic form factors f of each given atom at a position z inside the unit cell. It is possible to assume either a point position for an atom, or an extended, "flat"

position for a molecule (such as AMP), where one takes the form factor values, and spreads them out over a range Δz of the unit cell, still applying equation 5.5.

The simplest model is to consider the host $Cd_{0.85}PS_{2.7}$ layers at a distance of 19.6 Å from one another with no included guest molecule. For the positions of the host atoms, we put the Cd layer in the center, with P atoms 1.1 Å above and below, and S atoms 1.9 Å above and below the Cd layer [1]. The structure factors obtained are shown in Table 5.2 under the heading of "Host Alone".

A simple modification of this model is to add in $AMP_{0.5}$ as a flat molecule of constant electron density, located from 3.9 Å to 15.7 Å . These end-points leave a small space of about 0.6 Å between the end of the original host layer and the beginning of the AMP molecule. A small variation in the end-point position does not make a large difference in the calculated structure factor values. The actual expansion of the host layer spacing of 13 Å is longer than the longest dimension of AMP, and in fact a more realistic model will be presented further on. At present, the flat model is simply to approximate the effect of the guest molecule to get the general structure factor features. The values calculated for this flat AMP model are found in Table 5.2 under the column "Host + Flat AMP". It should be noted once again that the values derived from experiment are absolute values, and the comparisons should be made to the absolute values of the calculated F.

It should also be pointed out that, in order to compare the calculated and experimentally derived structure factors, the latter have been normalized to be on the same scale as the former.

The absolute values of F in Table 5.2 are plotted in Fig. 5.2.

While the agreement is not very good, particularly beyond the 5th order peak, this first model can be used as a guideline for further refinements. Thus, since both host alone and host + flat AMP give negative values for F_{005} and F_{006}, a 1-d electron density map can be calculated from the experimental F values, assuming that F_{005} and F_{006} are negative. Such an electron density map, for both B = 5 Å^2 and B = 10 Å^2, is shown in Fig. 5.3.

Fig. 5.3 shows a peak at 0, which corresponds to the layer of Cd atoms in the center of the unit cell. The next peak is located between the expected P and S positions, and it is not surprising that the P and S positions cannot be resolved. This is due to the limited resolution of this calculation of approximately 0.7 Å , since we have 14 peaks

Table 5.2: Structure factor values derived from experiment and calculated for host $Cd_{0.85}PS_{2.7}$ layers alone and for host $Cd_{0.85}PS_{2.7}$ layers with flat AMP molecules included between the layers.

Order of Peak	F for Host Alone	F for Host + Flat AMP	F from experiment (B = 5)
1	361	180	129
2	257	204	175
3	138	171	149
4	42.1	81.9	110
5	-12.4	-12.4	15.1
6	-3.46	-26.4	118
7	45.8	35.6	19.5
8	111	120	34.5
9	174	187	41.4
10	194	194	52.3
11	176	168	73.9
12	147	142	115
13	101	105	56
14	55.3	60.5	56

$\times$ 2 (due to the assumption of symmetry) for a region of 20 Å. Nevertheless, while the plot shown in Fig. 5.3 can suggest something about the arrangement of atoms in the unit cell, the unsatisfactory match between the modelled and experimentally derived structure factors shown in Fig. 5.2 needs to be addressed. In particular, the significant discrepancies in the 8th to 11th order peaks are rather insensitive to models that vary the placement of the guest AMP molecule. Thus, in order to bring the model closer to the structure factor from experiment, a re-examination of the host model is necessary.

One possibility is that the host layers undergo some buckling, or puckering, when they are no longer in their crystalline form. This type of behaviour is observed in single-layer MoS_2 and WS_2 suspensions [37]. Both of these layered materials have a somewhat similar structure to $CdPS_3$, where the metal atoms are arranged hexagonally in the plane, and are octahedrally coordinated (in their single layer form) to

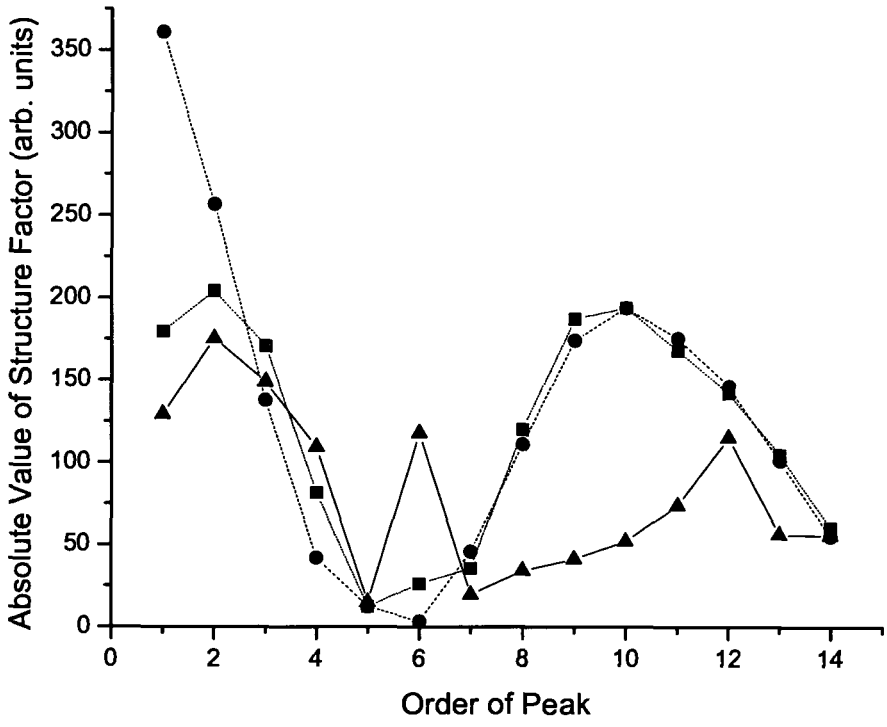

Figure 5.2: Comparison of absolute values of structure factor F for $Cd_{0.85}PS_{2.7}$ alone (circles), with flat AMP included (squares), and F from experiment with B=5 Å^2 (triangles).

sulfur atoms above and below the metal atoms. Thus it is worth investigating whether a buckling model would give a better agreement for structure factor with that derived from the experimental data for the $CdPS_3$ system.

The simple buckling model suggested here consists of Cd atoms, P atoms and S atoms in the host being displaced perpendicular to the original plane by $\pm x$ Å, with adjacent atoms (or rows of atoms) alternately being raised or lowered by the same amount x. The exact three-dimensional layout is not addressed in this one-dimensional model, but a possible arrangement will be displayed following the determination of the best fitting buckling value. Absolute values of structure factor for x = 0 and 0.2 Å are compared to F from experiment in Fig. 5.4, and x = 0.4 and 0.6

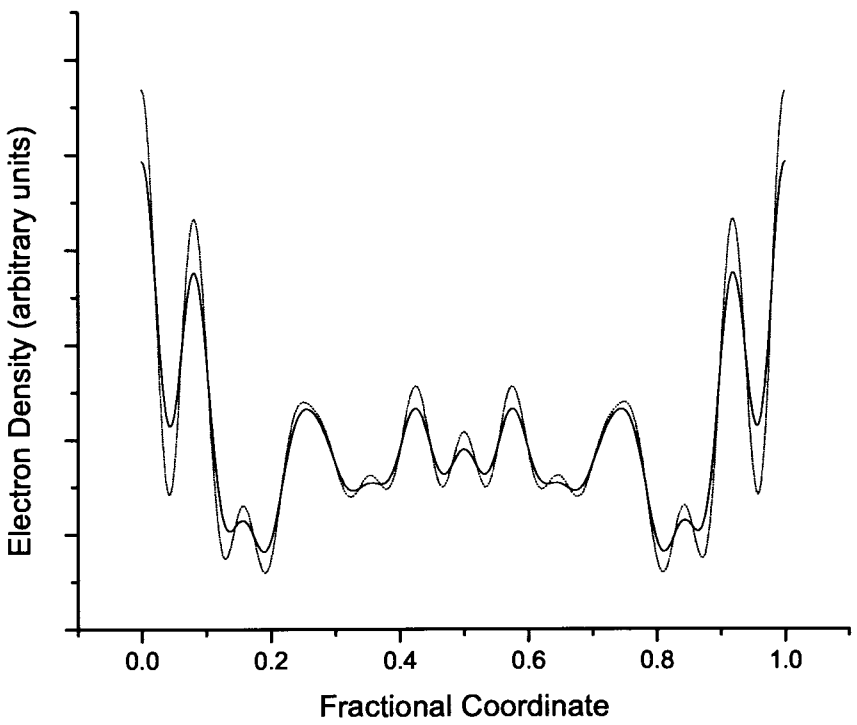

Figure 5.3: Electron density projection for $Cd_{0.85}PS_{2.7}(AMP)_{0.5}$, with negative F_{005} and F_{006}, with all other F_{00l} positive. F values are derived from experimental data, for B = 5 Å^2 (heavy line) and B = 10 Å^2 (light line).

Å calculations are compared to F from experiment in Fig. 5.5.

The agreement between the model with buckling of ± 0.6 Å is clearly the best of the buckling models shown in Figs 5.4 and 5.5, and a significant improvement over the previous calculations shown in Fig. 5.2. In comparison, the values calculated by Gordon et al. [37] for MoS_2, using an XAFS measurement, were a puckering for Mo atoms of ±0.23 Å and of S atoms of ±0.33 Å. Thus our value of ± 0.6 Å is significantly greater, but nonetheless the agreement is strongly suggestive of a puckering of this type occurring.

Figs. 5.6 and 5.7 demonstrate a possible model with a ± 0.6 Å buckling for a single layer of $CdPS_3$. Note that the Cd vacancies are not shown in the pictures. In

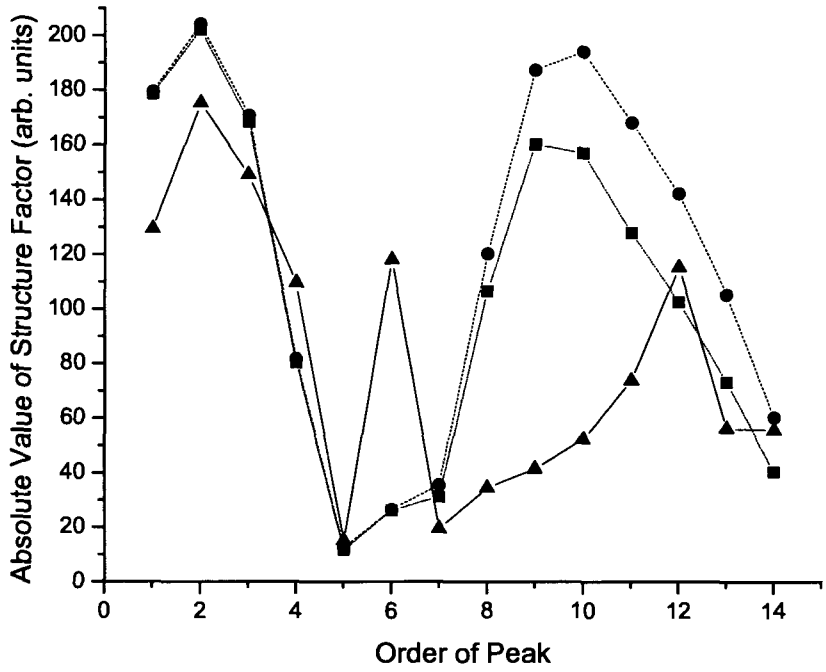

Figure 5.4: Comparison of absolute values of structure factor F for $Cd_{0.85}PS_{2.7}$ with flat AMP included. Circles are values with no buckling, squares are for buckling of ± 0.2 Å, and triangles show F from experiment with B=5 Å^2.

Fig. 5.7, the front row of atoms is lowered from its ideal central position by 0.6 Å, and the row immediately behind is raised by the same amount.

The structure factors calculated for the buckling model give negative values of F not only for the 5th and 6th order peaks, but also for those from $l = 9$ to $l = 14$. Applying these negative values to the structure factors calculated from the diffraction data for B = 5 Å^2 and for B = 10 Å^2 and shown in Table 5.1, we calculate the electron density map once again. These plots are shown in Fig. 5.8. The two plots are quite similar, which allows us to continue using B = 5 Å^2 for comparisons with models.

It should be noted at this point that upon truncating the series to 13 orders and ignoring the 14th, the electron density map looks nearly identical, except that the central region, between z = 0.4 and 0.6, is more smoothed out.

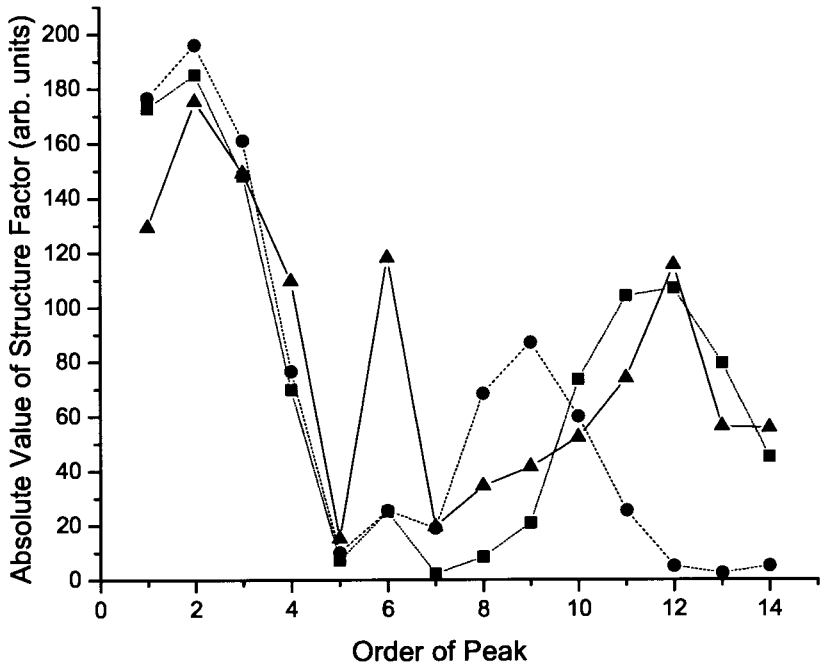

Figure 5.5: Comparison of absolute values of structure factor F for $Cd_{0.85}PS_{2.7}$ with flat AMP included. Circles are values with a buckling of ± 0.4 Å, squares are for buckling of ± 0.6 Å, and triangles show F from experiment with B=5 Å^2.

We can see that the electron density plots in Fig. 5.8 fit the buckling model of Fig. 5.7 for the host, where now there is a bit of a trough at z = 0, and two peaks on either side of 0 corresponding to the new Cd positions (as well as some of the P and S). Fig. 5.8 can also guide us to the possible orientation of the AMP molecule. The large peak centered at z = 0.26 should correspond to a region of high electron density, most likely the phosphate group and other atoms lined up together.

At this point it is worth reviewing what spacings other researchers have found for their AMP intercalates in layered double hydroxides. Choy and co-workers [2] found an interlayer expansion of 12.1 Å over the original host spacing, and Lotsch *et al.* [6] found a range between 11.8 and 12.7 Å in their systems. Interestingly, the latter also found that under vacuum, the guest spacing was reduced to 9.5 Å , and they suggest

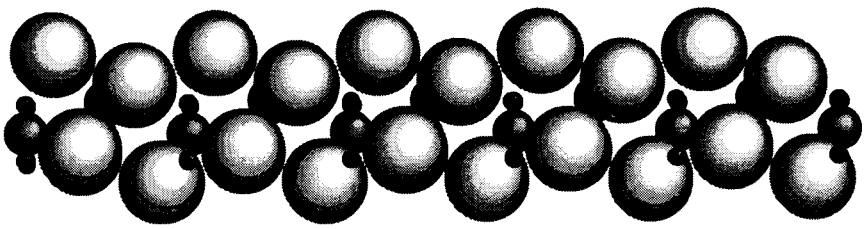

Figure 5.6: Side view (looking along the corrugations) of a model of a single layer of $CdPS_3$ showing a buckling of ± 0.6 Å. Medium gray circles are Cd atoms, small black circles are P atoms and large light gray circles are S atoms.

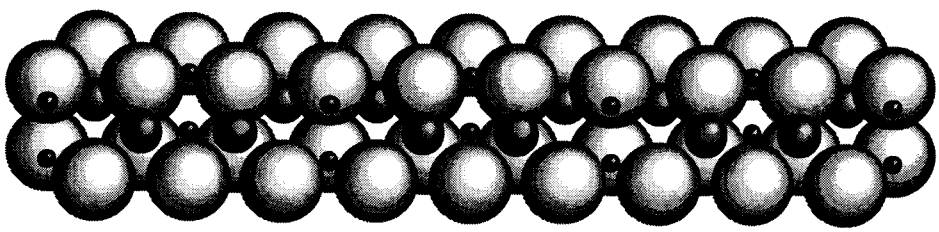

Figure 5.7: Front view (looking perpendicular to the corrugations) of a model of a single layer of $CdPS_3$ showing a buckling of ± 0.6 Å. Medium gray circles are Cd atoms, small black circles are P atoms and large light gray circles are S atoms.

that hydration is responsible for the difference.

In our $Cd_{0.85}PS_{2.7}(AMP)_{0.5}$ system, if we assume that the buckling model is correct, the host layer thickness becomes 1.2 Å greater than the original 6.5 Å, and we now assign a thickness of 7.7 Å to the host layer. This leaves 19.6 - 7.7 = 11.9 Å, in good agreement with the hydrated samples of Choy *et al.* and Lotsch *et al.* mentioned above. Given the 2.4 Å difference with the vacuum sample of Lotsch *et al.*, it is reasonable to assume that approximately one monolayer of water (nominally 2.8 Å in size) is included between the layers together with the AMP.

As mentioned above, the location of the large peak corresponding to high electron density in Fig. 5.8, at z = 0.26, or 5.1 Å from the center of the host layer, can be assumed to belong to phosphate and other groups of atoms in the AMP molecule. The location is too close to the host to allow for a water molecule bridging the host and the phosphate group. Instead, our model will place the water molecule at the

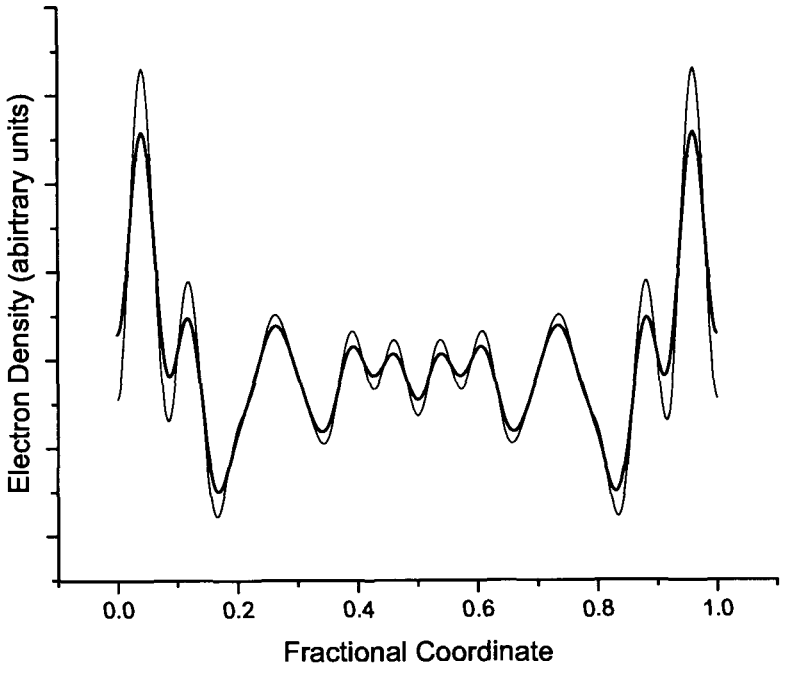

Figure 5.8: Electron density projection for $Cd_{0.85}PS_{2.7}(AMP)_{0.5}$ derived from experimental data, with B = 5 Å^2 (heavy line) and B = 10 Å^2 (light line). The signs of the structure factor values are determined for a host layer buckling of ± 0.6 Å.

other end of the AMP, associated with the N_1 nitrogen atom of the AMP, which is labelled in Fig. 5.9. Fig. 5.9 shows our model for the arrangement of the guest AMP and H_2O molecules, displayed in alignment with the peaks in the electron density map of Fig. 5.8 for B = 5 Å^2.

Keeping in mind that we have a certain amount of Li^+ in the system, it would seem that the Li^+ ions attach themselves directly to the phosphate group of the AMP, and are assumed to be near the host layers on either side of the Cd vacancies, as mentioned in the sample preparation section.

The assumptions that Li^+ is attached to phosphate, while a water molecule is associated with the N_1 atom in the AMP, are justified by the findings in the literature for AMP interactions with alkali metal ions and with water. In particular,

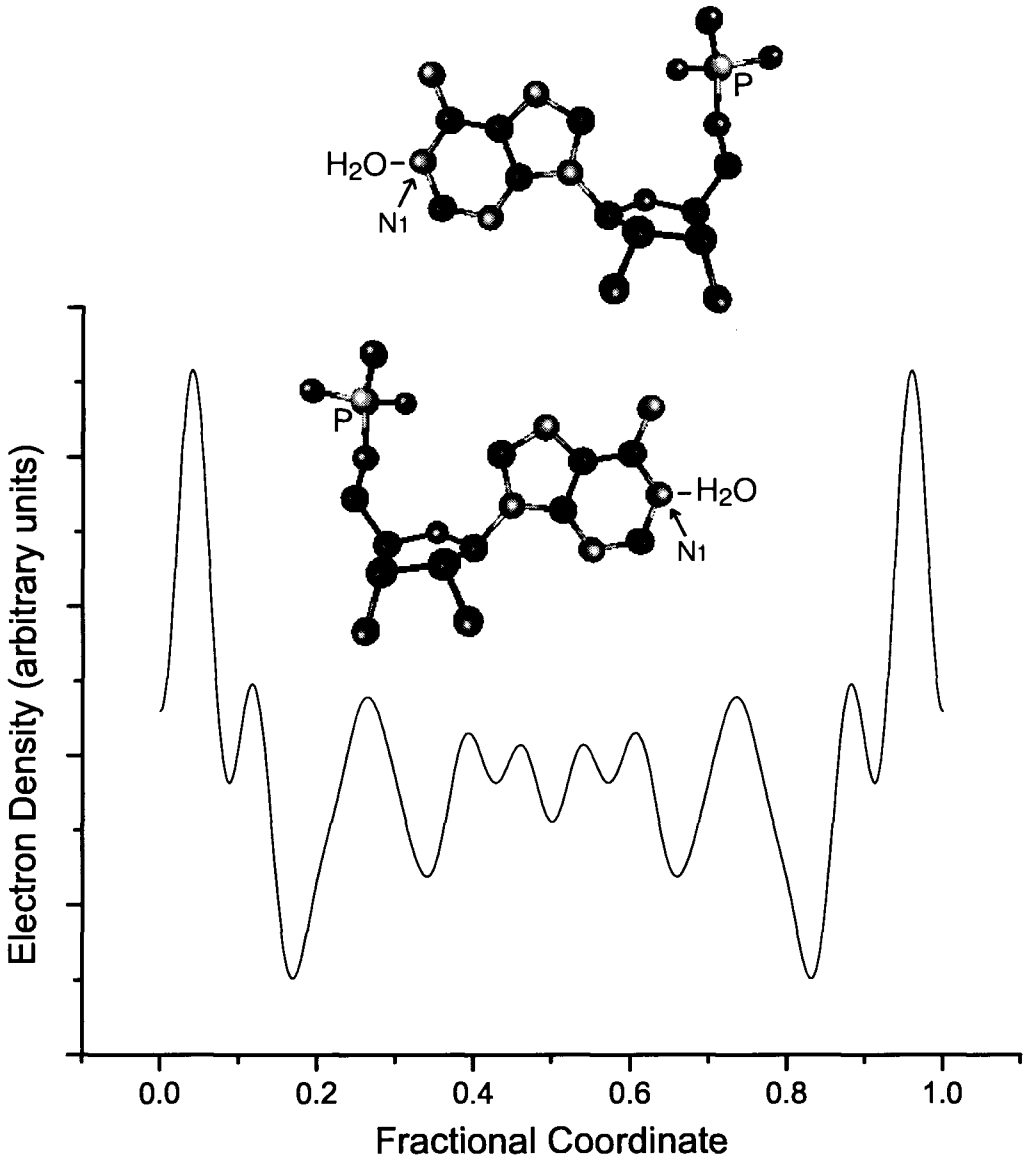

Figure 5.9: Model for the arrangement of AMP and H_2O overlaid on the electron density projection of $Cd_{0.85}PS_{2.7}(AMP)_{0.5}$ derived from experimental data, with B = 5 Å^2.

an infrared spectroscopy and nuclear magnetic resonance study by Tajmir-Riahi and Messaoudi[29] gives results that are pertinent to our model. They studied both solution and solid salt interactions of AMP with various ions, including alkali metal ions such as Li^+. Among their results were studies of AMP in solution with Li^+ ions, an environment similar to that of our samples with the $Cd_{0.85}PS_{2.7}$ single layer suspensions. Their findings suggest that since the N_1 atom in the acid form of AMP (which is the form used in this work) is protonated, it is likely to form a bond with water. They also found that, unlike for the other alkali metal ions, Li^+ appears to attach itself directly to the phosphate group without an intervening water molecule. These results are consistent with our model presented above.

Further consideration of Fig. 5.9 suggests some refinements to the flat AMP models considered earlier in this section. Groups of atoms are considered separately, spread over smaller regions of the interlayer space. Also, the P atom is counted as lying at the point z = 0.26. The positions of various groups of atoms in the model are summarized in Table 5.3. It should be noted that for every atom or group of atoms at position z, the same group appears at 1-z. This is not shown in Table 5.3.

It should also be noted that while the H atoms are not shown in Fig. 5.9, their small contribution to electron density is included in Table 5.3 and all structure factor calculations.

Table 5.3: Positions of groups of atoms belonging to the guest molecules AMP and H_2O in $Cd_{0.85}PS_{2.7}(AMP)_{0.5}$, arranged as suggested by the model of Fig. 5.9.

Fractional Coordinate	Coordinate (Å)	Atoms
0.18 - 0.23	3.5 - 4.5	OH
0.23 - 0.33	4.5 - 6.5	$C_3O_4H_5$
0.26	5.1	P
0.33 - 0.49	6.5 - 9.6	$C_3O_2N_2H_4$
0.51 - 0.64	10.0 - 12.5	$C_4N_3H_3$
0.64 - 0.78	12.5 - 15.3	H_2O

In Fig. 5.10, the structure factor values calculated from the atom positions shown in Table 5.3 and the buckled host are compared with the experimentally derived F,

and with the F values calculated for a model with buckled host but only flat AMP inside.

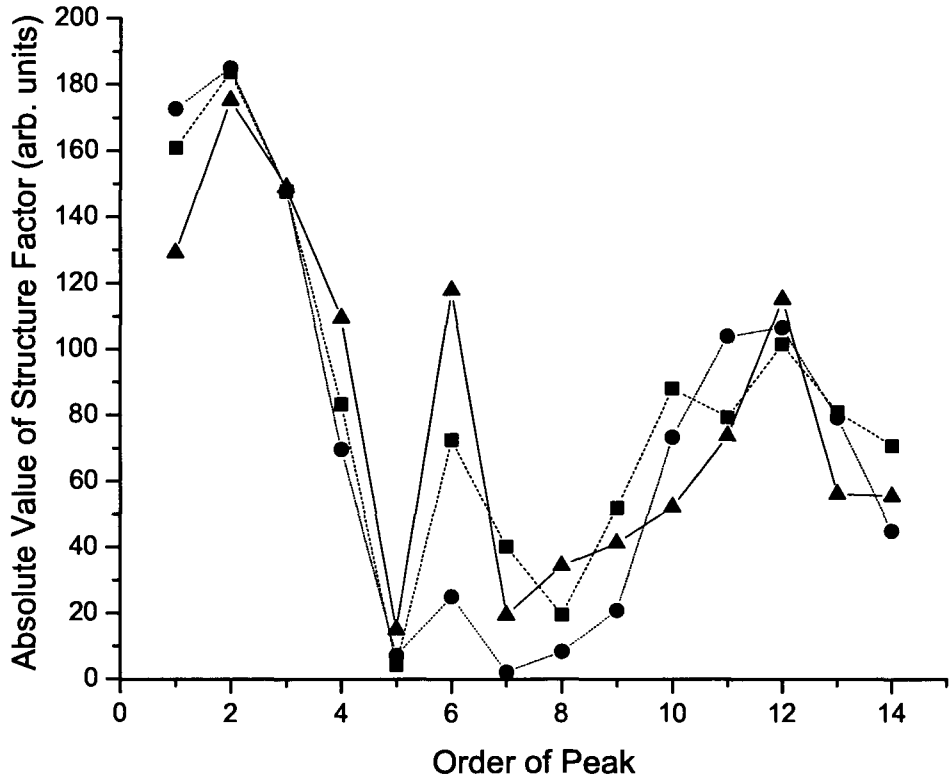

Figure 5.10: Comparison of absolute values of structure factor F for $Cd_{0.85}PS_{2.7}$. Triangles show F from experiment with B=5 Å^2, circles show a $\pm$ 0.6 Å buckled host with flat AMP included, and squares show a $\pm$ 0.6 Å buckled host with guest molecules according to the model of Fig. 5.9 and Table 5.3.

Two interesting features are apparent in Fig. 5.10. First, the detailed model is much closer than the flat model to predicting the strong value of F_{006}, which is one of the striking features of the X-ray diffraction pattern shown in Fig. 5.1. The second interesting note about the comparison shown in Fig. 5.10 is that, other than F_{006}, there is no significant improvement in the detailed model over the flat AMP model.

This suggests that the z=0.26 peak, which is related to the strength of the F_{006} value, cannot be ignored. At the same time, the electron density in the middle of the system, between around z=0.3 and z=0.7, is rather spread out and insensitive to detailed placement of atoms.

5.3 XRD peak width analysis of $Cd_{0.85}PS_{2.7}(AMP)_{0.5}$

Studying the peak widths from X-ray diffraction can give us insight into the coherence size and ordering of the sample in the direction perpendicular to the planes.

Peak width is influenced by two main factors. For one of these factors, commonly referred to as the coherence length, the greater the number of planes stacked regularly, the narrower the diffraction peak. Broad peaks would be a result of, for example, small domain size for crystal powders, while large domain size gives rise to narrow peaks. This type of broadening or narrowing affects all peaks in the same way, regardless of the order n of the peak.

A second factor influencing broadening, this time affecting high order peaks more significantly than low order peaks, is displacement disorder of the second kind [38]. This name is given to distinguish it from displacement disorder of the first kind, which is usually due to thermal vibrations, as mentioned in the electron density section. Displacement disorder of the first kind does not cause peak broadening, though it does cause a reduction of intensity for high order peaks. Displacement disorder of the second kind, on the contrary, causes peak broadening without loss of intensity.

In displacement disorder of the first kind, the average position of the scattering centers is not a function of distance from the origin, since individual scatterers fluctuate about their own average position, but the average position itself is regular. Thus there is no loss of long-range order. However, in displacement order of the second kind, there is a loss of long-range order, because the average position of the scatterer can actually change over long range. Instead of fluctuations cancelling out to maintain an average position that is always a multiple of the distance from one unit cell to the next, the fluctuations accumulate, thus destroying long-range order. Another way to describe displacement disorder of the second kind is that there is a (usually

narrow) distribution of average positions, instead of just one value. Referring back to Fig. 5.1, it is clear that the high order peaks are broader than the low order peaks. Therefore displacement disorder of the second kind appears to be playing a role in the broadening of the peaks.

According to Guinier [38], an approximate formula that takes into account both of the contributions to peak width w mentioned above, namely coherence length and long-range disorder, is given by the following equation:

$$w = \sqrt{(\frac{1}{Nd})^2 + (\delta s)^2}. \tag{5.6}$$

The first quantity is the coherence length broadening. Applied to our oriented films, N is the number of coherent layers, and d is the average basal plane spacing. δs is the part of the width due to the disorder broadening, and is defined as follows:

$$\delta s = \frac{1}{d}\pi^2 n^2 (\frac{\Delta}{d})^2. \tag{5.7}$$

Δ is a parameter giving a measure of the disorder, with units of length and n is the order of the peak.

We can apply the peak widths measured from Fig. 5.1 to equations 5.6 and 5.7 in order to extract the coherence length and the disorder parameter Δ. In Fig. 5.11, a fit of the theoretical peak widths to the experimentally determined widths is shown. Due to the low intensity of the (005) and (007) peaks, it is difficult to estimate the width of these peaks accurately, and they are left out of Fig. 5.11. Error bars for the other peak widths also arise from confidence in measuring the widths.

Two fits are shown in Fig. 5.11, one to N = 14 and Δ = 0.195 Å (triangles), and the other to N = 18 and Δ = 0.19 Å (circles). Both models have a similar value for Δ, and we can take 0.19 or 0.195 Å as values that fit the measured peaks quite well. The Δ value is largely determined by the higher order peaks.

However, in calculating a value for the number of coherent layers N, mainly determined by the low order peaks, the widths of the 1st and 2nd order peaks are not consistent with those of the 3rd, 4th and 6th order peaks according to the proposed equation. The n = 1 and 2 peaks give a value for N of 18 layers, while the n = 3, 4 and 6 peaks give a value for N of 14. Thus the coherence length is not easy to determine unambiguously. Nevertheless, it is clear that N lies between 14 and 18 layers for this

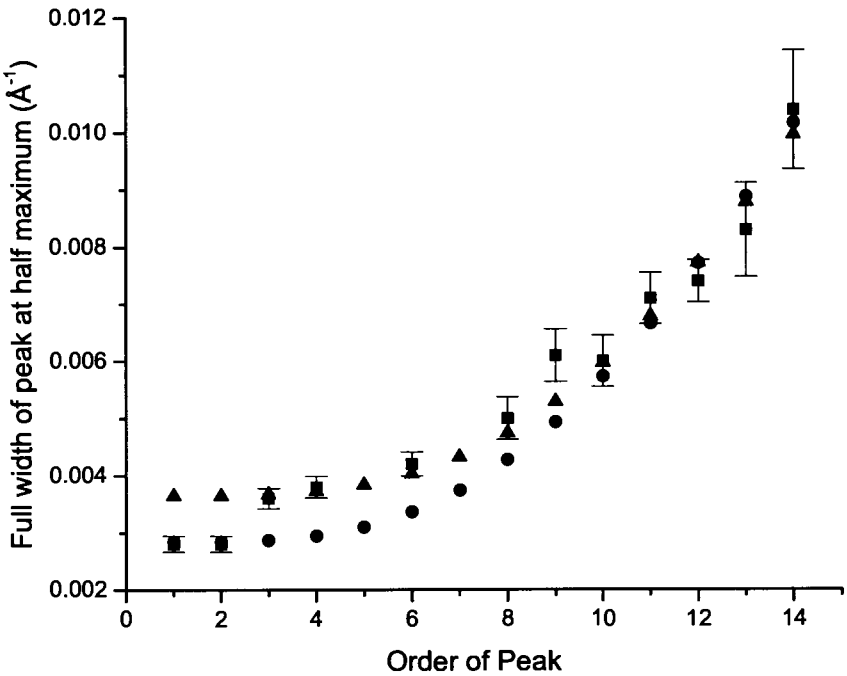

Figure 5.11: Width of XRD peaks and fits to theory for $Cd_{0.85}PS_{2.7}(AMP)_{0.5}$. Squares with error bars represent the widths from experiment. Circles correspond to a fit with a coherence length of 18 layers (≈350 Å) and a disorder parameter Δ of 0.195 Å, and triangles correspond to a fit with a coherence length of 14 layers (≈275 Å) and a Δ of 0.19 Å.

sample, or between about 275 and 350 Å.

To summarize, we can assign a value of 0.19 Å for Δ, and between 275 and 350 Å for the coherence length. This shows that the sample is highly ordered, when one considers that 0.19 Å is only about 1% of the 19.6 Å basal plane spacing of the sample.

5.4 pH of protonation

In the Introduction, it was mentioned that base nitrogens of AMP and CMP undergo an additional protonation below a pH of 3.88 for AMP, and 4.54 for CMP [19]. Since the typical pH of sample suspensions prior to forming films is around 4-4.5, AMP does not become protonated, while CMP does. An investigation of the pH effect on the $Cd_{0.85}PS_{2.7}(AMP)_{0.5}$ system was undertaken in order to determine whether the additional protonation during preparation of the suspensions could have some influence on the sample's response to humidity.

A pair of samples was prepared, one concentrated, with a pH of 3.5, and the other more dilute, with a pH of 4.5. The ratio of $CdPS_3$ to AMP was kept the same for both samples. The two suspensions had a similar appearance, with no sign of flocculation. Upon drying, XRD patterns of the films were taken over a range of RH, and were found to be quite similar. Two pairs of these patterns are shown in Figs. 5.12 and 5.13.

The XRD patterns in Fig. 5.12 show that at 4-5 % RH, the two samples are dominated by the same phase with a spacing of 19.3 Å (calculated from the second-order peak positions), close to the 19.6 Å spacing that was observed for the sample in Fig. 5.1. The first-order peaks are not perfectly aligned, but that appears to be partly due to the shoulder appearing in the pattern for the sample prepared at pH 3.5, and perhaps partly due to a slight misalignment of the sample height, which affects the low angle peaks. The second, third and fourth order peaks are better aligned, so on the whole it can be said that the two samples do not show significant differences at this relative humidity.

In Fig. 5.13, the two samples are shown at 61 % (pH 3.5) and 66 % RH (pH 4.5). Again, other than a shoulder for the sample prepared at pH 3.5, the two sets of peaks match up (even the first-order peaks). In this case, the plane spacing is 19.8

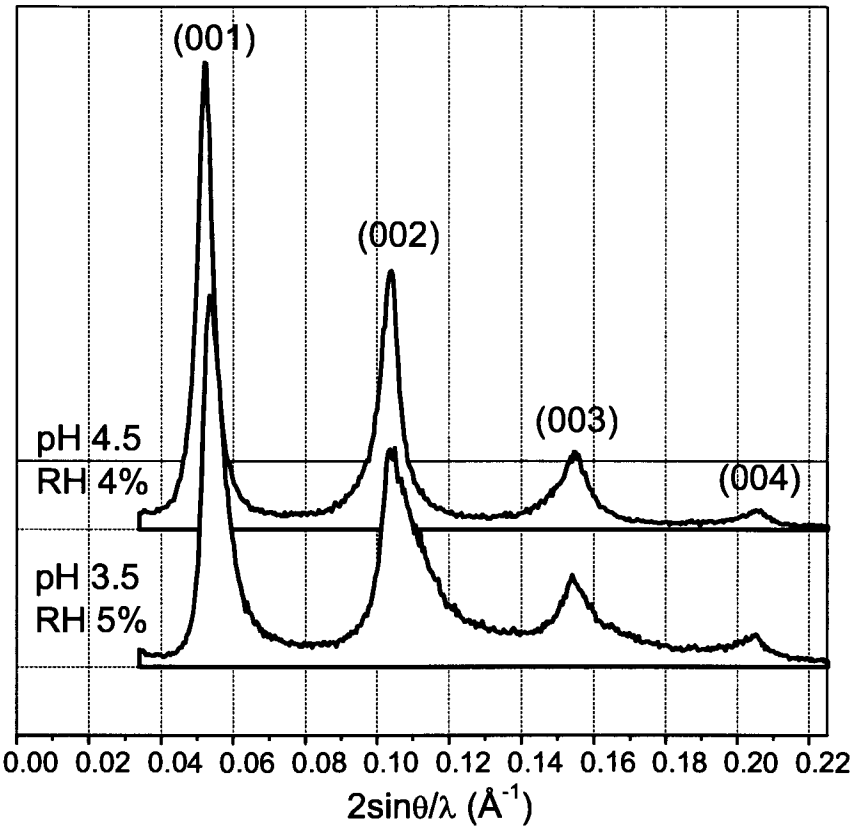

Figure 5.12: X-ray diffraction patterns for oriented films of $Cd_{0.85}PS_{2.7}(AMP)_{0.5}$ at 21 ± 1 °C. The upper, taken at 4% RH, is for a sample prepared at pH 4.5; the lower, taken at 5% RH, was prepared at pH 3.5.

Å, confirming the statement made in chapter 4 that the spacing of the AMP samples does not change significantly with humidity at low ranges.

It is perhaps not too surprising that the initial pH of the suspension does not have a significant effect on the structure of the restacked films, since as the films are formed, water evaporates from the system, and presumably in the end the dilute sample passes through a more concentrated state before the $CdPS_3$ layers restack with the AMP included. In that case, since the initial ratio of $CdPS_3$ to AMP is the same, the two samples end up in the same state. Nevertheless, the results of this experiment demonstrate that the extra protonation that occurs in CMP, but not in

AMP, during sample preparation does not have an influence on the structure or on the response to humidity of the restacked films. Indeed, earlier in this chapter, it was already assumed that the N1 atoms in the AMP molecules are protonated in the restacked films regardless of the initial pH of the suspension. The results presented in Figs. 5.12 and 5.13 tend to confirm this possibility.

5.5 Intercalation of NMPs into $K_{0.4}Cd_{0.8}PS_3(H_2O)_y$

In chapter 2, it was noted that the sample preparation involved restacking suspensions of single layer $Cd_{0.85}PS_{2.7}$ in the presence of NMPs dissolved in water. The question arises of whether exfoliation of $CdPS_3$ is necessary for the formation of the inclusion compounds with NMP. In an attempt to verify the importance of exfoliation in the formation of $CdPS_3$/NMP samples, an intercalation was attempted with solutions of CMP and AMP into $K_{0.4}Cd_{0.8}PS_3(H_2O)_y$ powder. Intercalation of a wide variety of molecules, including organic molecules and polymers, has been discussed by a number of workers, as mentioned in the review by Grasso and Silipigni [14].

In the present work, the combined CMP or AMP and $K_{0.4}Cd_{0.8}PS_3$ were stirred for 18 hours, dropped on glass slides and allowed to dry in air.

The XRD pattern of the AMP sample is shown in Fig. 5.14. The pattern is quite similar to the one shown in Fig. 5.1, which was obtained from a sample prepared from a restacked suspension. The relative humidity was around 40 %. It is quite clear that the AMP intercalation was successful.

On the other hand, the CMP intercalation was unsuccessful. In the case of CMP, the resulting pattern showed only the original $K_{0.4}Cd_{0.8}PS_3(H_2O)_y$ peaks, together with a small peak showing restacked $CdPS_3$ with nothing included. The difference will be revisited in the Discussion and Conclusions chapter.

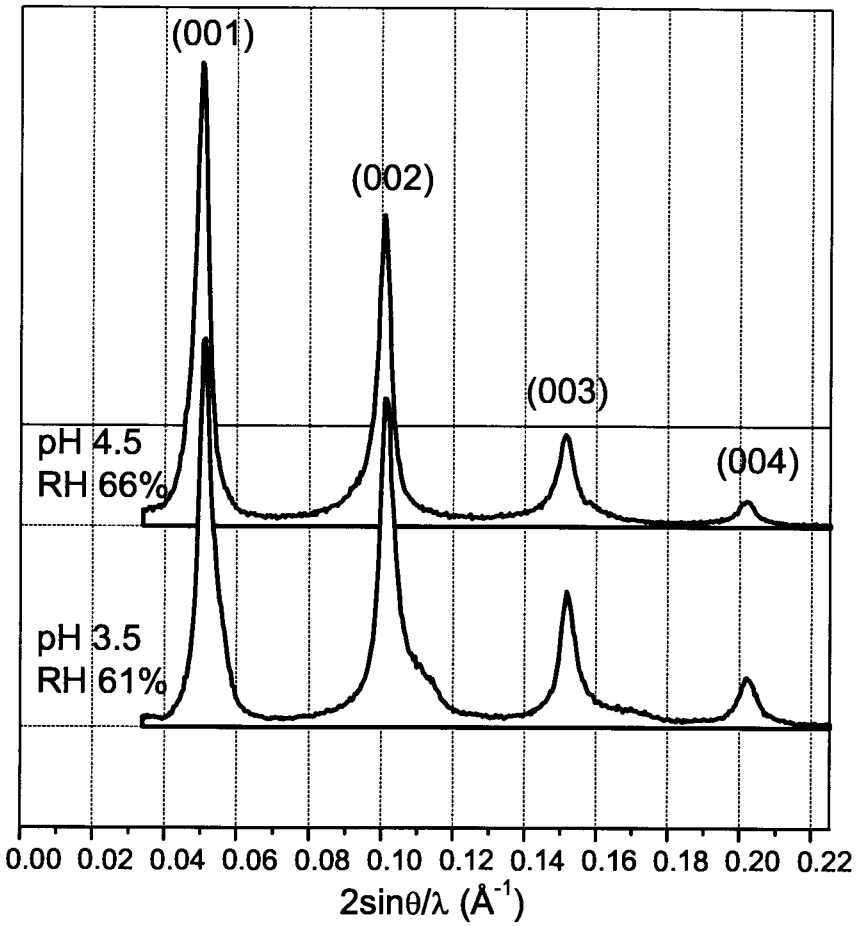

Figure 5.13: X-ray diffraction patterns for oriented films of $Cd_{0.85}PS_{2.7}(AMP)_{0.5}$ at 21 ± 1 °C. The upper, taken at 66% RH, is for a sample prepared at pH 4.5; the lower, taken at 61% RH, was prepared at pH 3.5.

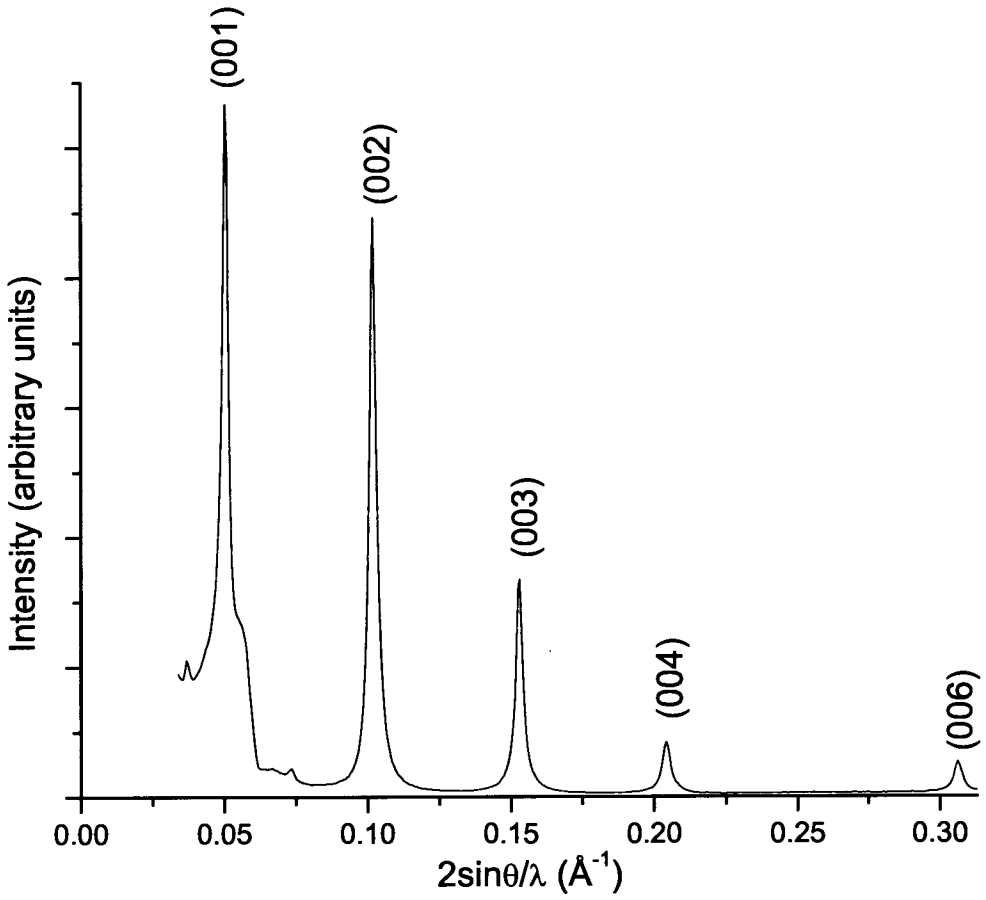

Figure 5.14: X-ray diffraction pattern for $K_{0.4}Cd_{0.8}PS_3(AMP)_x(H_2O)_y$ at room temperature and RH about 40 %.

Chapter 6

X-ray Diffraction Studies of $Cd_{0.85}PS_{2.7}(CMP)_{0.3}$

The studies of XRD patterns for the CMP samples will focus on their response to changes in relative humidity, which are more dramatic than those of the AMP samples discussed in the last chapter, particularly in the range of 0 - 80 % relative humidity.

It is useful to first establish a spacing for a fully dehydrated sample. In order to drive off the water that is contained in the sample, one film of $Cd_{0.85}PS_{2.7}(CMP)_{0.3}$ was heated to 80 °C. The XRD pattern of this sample is shown in Fig. 6.1. A host plane spacing of 14.8 Å is calculated from this pattern, corresponding to an expansion of 8.3 Å over the unintercalated $CdPS_3$. This expansion is compatible with the size of a CMP molecule with no associated water. We can take this spacing to be the "dry" spacing for this compound, and as we shall see, at room temperature, even at 2 % humidity, this dry spacing is not favoured.

Figs. 6.2 and 6.3 show a series of XRD patterns for another sample of $Cd_{0.85}PS_{2.7}(CMP)_{0.3}$ at room temperature (21±1°C) over a range of relative humidities from 0 to 82 %. Each pattern took about 20 minutes to record, and a minimum of 20 minutes elapsed after each new humidity step was reached. A delay of longer than 20 minutes did not appear to affect the patterns.

Fig. 6.2 displays a series of patterns with increasing humidity, while Fig. 6.3 shows a series with decreasing humidity. There are several features to point out in these patterns.

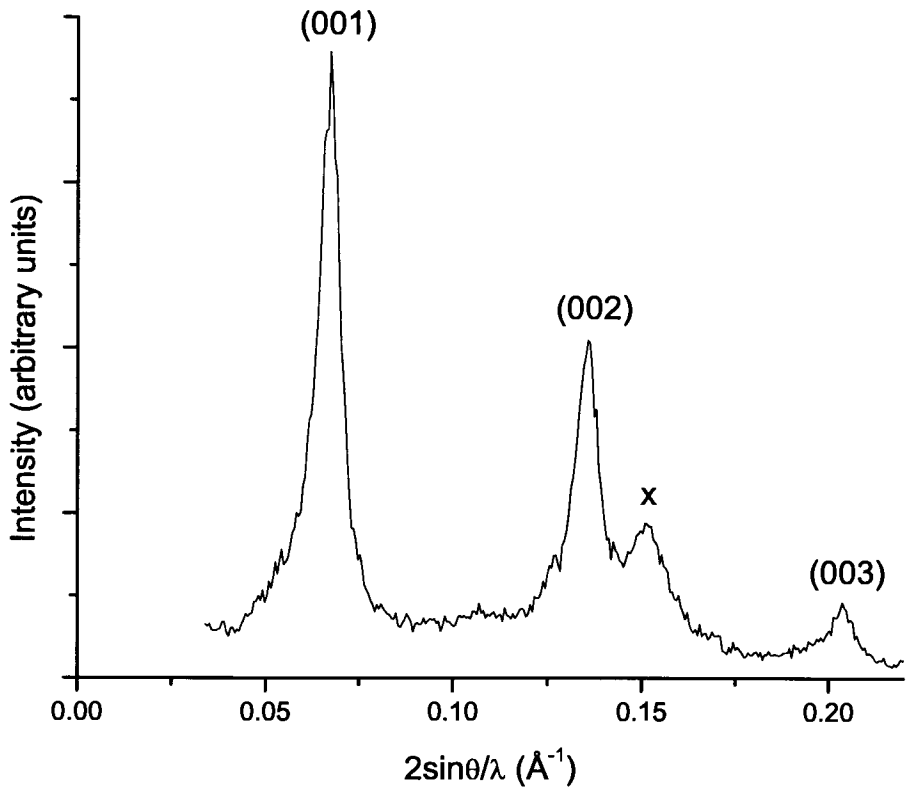

Figure 6.1: X-ray diffraction pattern for a fully dehydrated oriented film of $Cd_{0.85}PS_{2.7}(CMP)_{0.3}$ at 80 °C. The x indicates a restacked $CdPS_3$ peak.

First, for both figures, the humidity step from one pattern to the next is typically around 2 %. However, there are some gaps and some steps of 1 % or 3 %. Therefore the relative humidity scale on Figs. 6.2 and 6.3 is approximately linear, but the numbers refer to the specific RH at which a particular pattern was run. Thus, for example, in Fig. 6.2, there is a pattern at 32 %, and the next are at 34 %, 37 %, 38 %, 41 %, 43 %, etc.

Second, there are three sets of peaks, corresponding to three different host plane spacings in the sample, in Fig. 6.2, labelled A, B and C. The numbers refer to the order of the peak, thus peak A2 is the (002) peak belonging to phase A. Phase C, with a spacing that varies from 14.3 to 15.1 Å with increasing humidity, disappears completely above about 65 % RH, and does not return upon decreasing humidity in

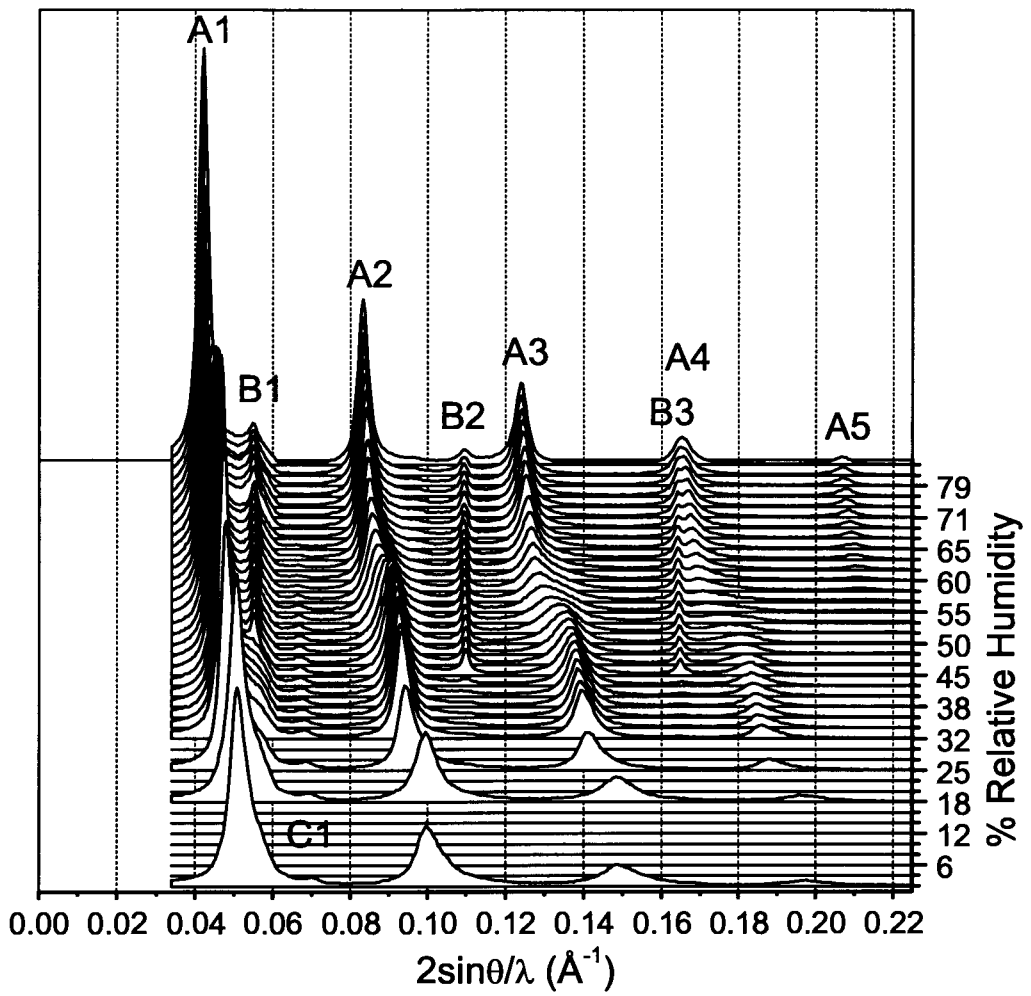

Figure 6.2: X-ray diffraction patterns for an oriented film of $Cd_{0.85}PS_{2.7}(CMP)_{0.3}$, with increasing relative humidity from 0 % to 82 %, at 21 ± 1 °C.

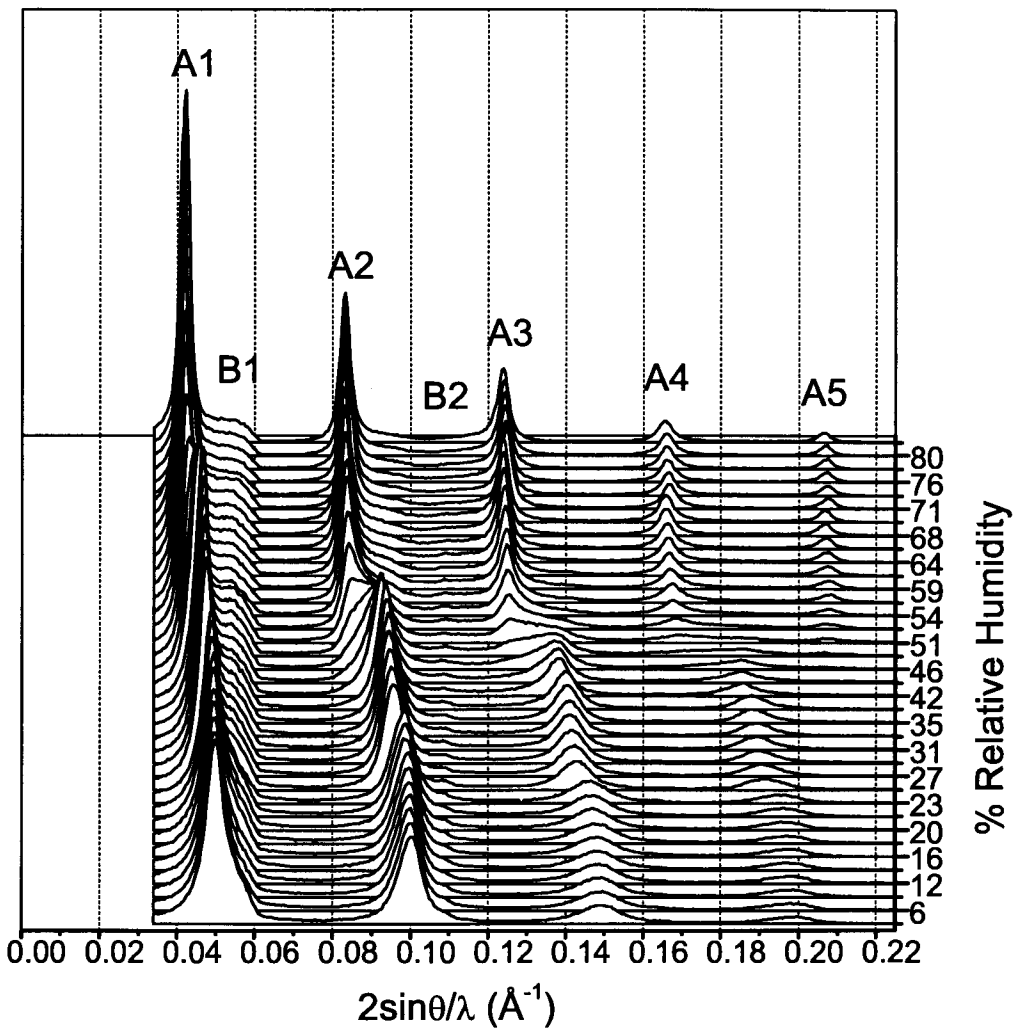

Figure 6.3: X-ray diffraction patterns for an oriented film of $Cd_{0.85}PS_{2.7}(CMP)_{0.3}$, with decreasing relative humidity from 82 % to 0 %, at 21 ± 1 °C.

Fig. 6.3. This phase has the same spacing as the dry phase of the pattern in Fig. 6.1. The fact that this is a small minority phase, and that it does not return even upon the RH decreasing back to 2 %, suggests that at least some water is quite stably bound to the CMP within the $CdPS_3$ layers, and that the dry phase of Fig. 6.1 is not easily obtained at room temperature.

The peaks of phase B, with a spacing ranging from 18.0 to 18.4 Å, are sharper than those of phase A in certain patterns, and do not change significantly in position as a function of RH. Their intensities are considerably less than those of phase A, meaning that phase A dominates most of the sample. Phase B is also somewhat reduced in intensity and the peaks are broadened after the 82 % RH level is reached, and on the way back down. It should be noted that XRD patterns for other samples of $CdPS_3$/CMP, not shown here, also tended to have multiple phases. While relative intensities between the peaks of different phases varied from sample to sample, the one examined in Figs. 6.2 and 6.3 is typical of the $CdPS_3$/CMP system.

The third point of interest in these patterns is the dependence of the spacing of phase A on relative humidity. Below about 25 % RH, there is very little change in the initial spacing of 19.0 - 19.3 Å (expansion over the original host of 13.5 - 13.8 Å). There is a significant change in spacing observable at around 50 % RH in both sets of patterns. There is also a smaller jump around 25 %. For the rest of the range between about 25 % and 70 %, there appears to be a roughly linear shift in the spacing with humidity. A calculation of this linear shift in the regions with no jumps in spacing yields a value of $2.4 \pm 0.2 \times 10^{-4}$ Å^{-1} per % RH for the (003) peaks, corresponding to an increase or decrease in plane spacing of around 0.045 Å per % RH. The small jump at around 25 % RH is not observed in another sample of $Cd_{0.85}PS_{2.7}(CMP)_{0.3}$, where the linear shift continues down to 2 % RH (data not shown). Between about 70 % RH and 82 % RH, the spacing levels off at around 23.9 Å for both sets of patterns, corresponding to an expansion of 17.4 Å. Thus in total, phase A increases in spacing by 3.9 Å from 2 % to 82 % RH.

On top of the linear shift between 25 % and 70 % RH, the large change in spacing at around 50 % RH can be thought of as a phase transition, where enough water gets into the system that the conformation of CMP changes to accomodate additional water and forms a new phase. The nominal size of a water molecule, 2.8 Å, is larger than the spacing change of the transition, so it is not a simple matter of a water layer

being formed parallel to the layers. A closer study of the jump region, 49 % to 60 % RH for the increasing humidity system of Fig. 6.2, and 56 % to 42 % RH for the decreasing humidity system of Fig. 6.3, can test and quantify this phase transition hypothesis.

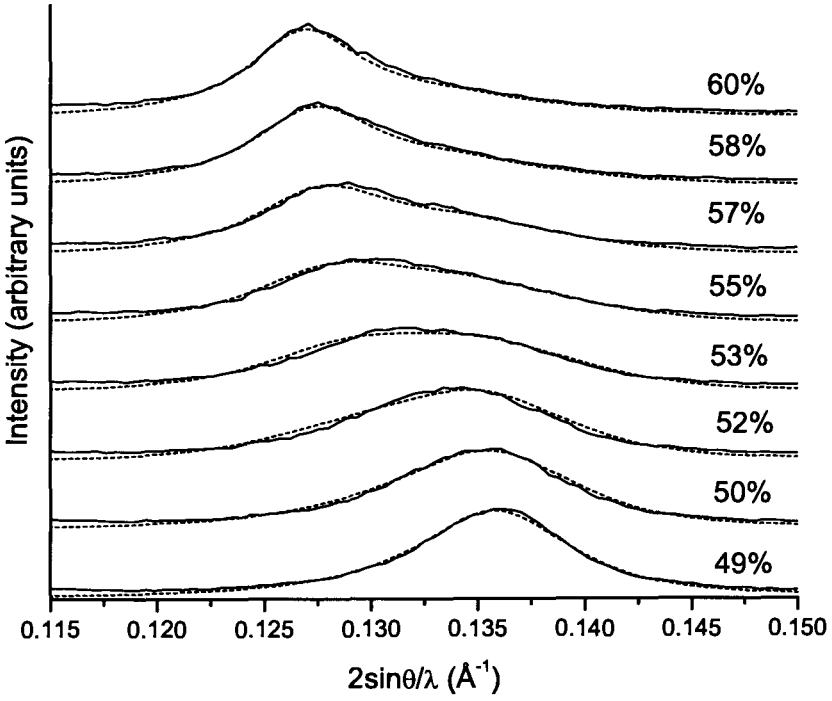

Figure 6.4: Pseudo-Voigt function fits to (003) peaks for the X-ray diffraction patterns of an oriented film of $Cd_{0.85}PS_{2.7}(CMP)_{0.3}$, with increasing relative humidity from 47 % to 60 %, at 21 ± 1 °C. The data are indicated by the solid line, and the mathematical fits by the dashed line.

The data for the (003) peaks (labelled A3) in Figs. 6.2 and 6.3 in the humidity ranges specified above were fitted to pseudo-Voigt functions, as shown in Figs. 6.4 and 6.5. These functions are in common use for modelling XRD peak shapes, and combine Lorentzian and Gaussian functions. The Lorentzian function can be expressed by the following equation:

$$f(x) = \frac{1}{s\pi[1 + (\frac{x-t}{x})^2]}, \tag{6.1}$$

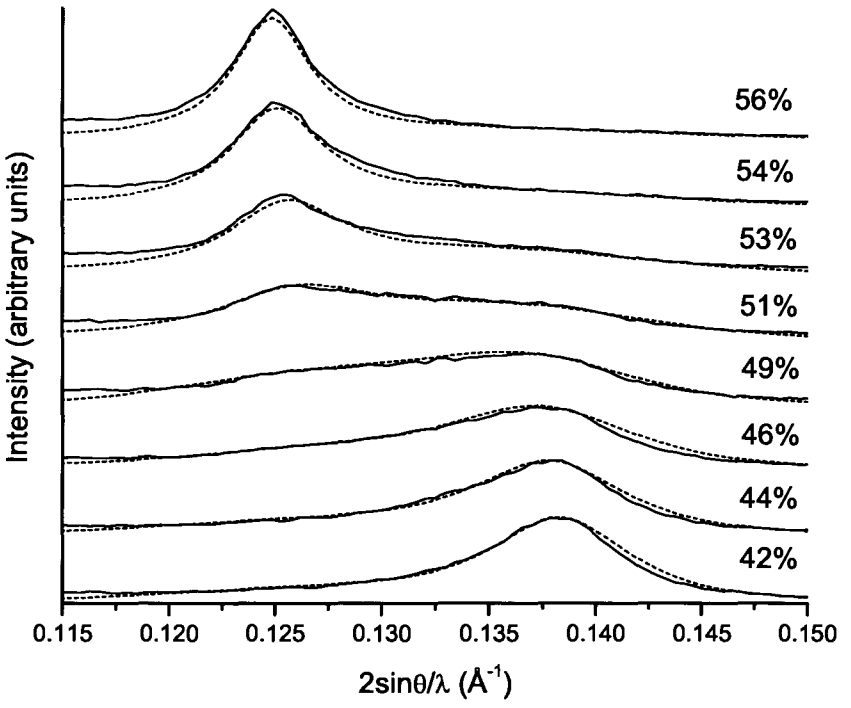

Figure 6.5: Pseudo-Voigt function fits to (003) peaks for the X-ray diffraction patterns of an oriented film of $Cd_{0.85}PS_{2.7}(CMP)_{0.3}$, with decreasing relative humidity from 56 % to 42 %, at 21 $\pm$ 1 °C. The data are indicated by the solid line, and the mathematical fits by the dashed line.

where s is the half width at half maximum, and t is the position of the peak centre. The Gaussian function is given by the following equation:

$$f(x) = \frac{1}{\sigma\sqrt{2\pi}} \exp[\frac{-(x-\mu)^2}{2\sigma^2}]. \tag{6.2}$$

Here, the half width at half maximum is given by $\sqrt{2\ln 2}\sigma$, or 1.177 σ, and μ is the position of the peak centre.

The pseudo-Voigt function is a weighted sum of the Lorentzian and Gaussian functions. The ratio is determined by the fitting program in the fits shown below. The mathematical functions at each point in RH are added and compared to the original data for increasing humidity in Fig. 6.4, and for decreasing humidity in Fig. 6.5. These

figures clearly show a good fit between the fitted functions and the data.

The fits are decomposed into two independent peaks in Figs. 6.6 and 6.7. The (003) peaks are chosen over (002) or (001) because the two distinct peak positions in the transition are sufficiently far apart to make fitting convenient. In addition, the (003) peaks have a greater signal to noise ratio than the (004) peaks. The position of the left-hand peak in the pair, corresponding to a higher plane spacing, is found from the position of the peak at an RH just above the range considered (i.e. for the pattern following the last one in the range). Similarly, the position of the right-hand peak is found from the position of the peak for the pattern corresponding to RH just below the bottom of the range. The fitted peaks are fixed to these positions, with allowance made for the linear shift discussed above as the RH changes. Aside from the fixed position, the least-squares fitting routine was allowed to freely pick peak widths and ratios of Gaussian to Lorentzian peak shape for each peak.

It is clear from the fits in Figs. 6.6 and 6.7 that one phase fades out as the other picks up in intensity. The peak widths are also changing - as one phase fades out, its peak widths get larger, while the peaks of the phase that takes over get narrower. As mentioned in the previous chapter, this makes sense in terms of peak width as a measure of coherence length. We can imagine domains of one phase getting smaller, and thus having a lower coherence length, as the humidity changes. Meanwhile, the other phase is getting larger domains, so its peaks are narrowing. The changes in peak area and width for the regions studied, as calculated from the fitting functions, are displayed in Table 6.1. The numbers demonstrate the trend of decreasing area with increasing peak width as a phase fades away. It is also worth noting that the total area is approximately constant, which implies that the entire phase A is shifting from one spacing to the other.

There are some interesting differences between the phase change of Figs. 6.6 and 6.7. In Fig. 6.6, which represents the increasing humidity patterns, the jump in spacing from one peak position to the other is about 1.1 Å. However, the jump for decreasing humidity shown in Fig. 6.7 is about 1.8 Å.

Regardless of this difference, as mentioned above, at the top and bottom of the humidity range from 0 to 82 %, both the increasing and decreasing patterns converge to the same spacings. A summary of the spacings for phase A is shown in Fig. 6.8. For the phase transition regions, the numbers are those used in the calculated fits.

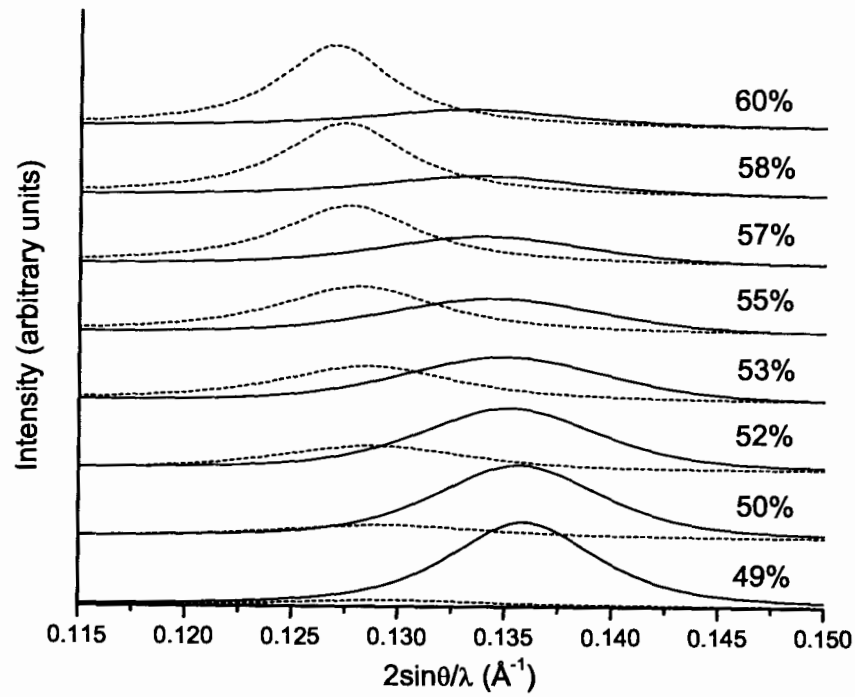

Figure 6.6: Pseudo-Voigt function fits to (003) peaks for the X-ray diffraction patterns of an oriented film of $Cd_{0.85}PS_{2.7}(CMP)_{0.3}$, with increasing relative humidity from 47 % to 60 %, at 21 $\pm$ 1 °C. The fits show the discrete change of phase with increasing humidity.

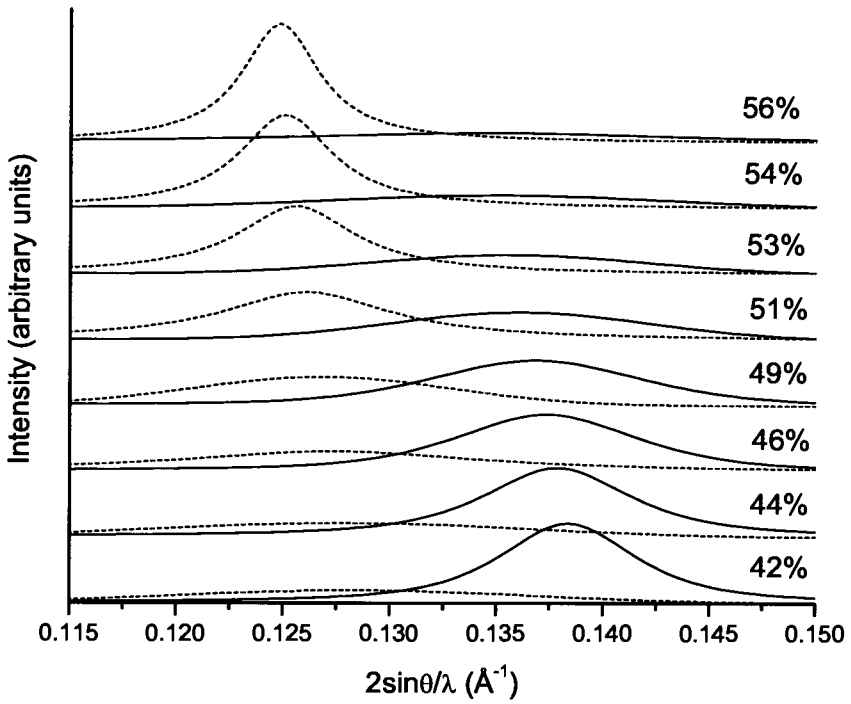

Figure 6.7: Pseudo-Voigt function fits to (003) peaks for the X-ray diffraction patterns of an oriented film of $Cd_{0.85}PS_{2.7}(CMP)_{0.3}$, with decreasing relative humidity from 56 % to 42 %, at 21 $\pm$ 1 °C. The fits show the discrete change of phase with decreasing humidity.

Table 6.1: Peak areas and widths for (003) peaks of $Cd_{0.85}PS_{2.7}(CMP)_{0.3}$ as calculated from the fitting functions displayed in Fig. 6.6 and Fig. 6.7, showing the phase shifts with increasing and decreasing relative humidity, respectively.

Increasing Humidity

% Relative Humidity	Left-hand peak area (arb. units)	Right-hand peak area (arb. units)	Left-hand peak width ($Å^{-1}$)	Right-hand peak width ($Å^{-1}$)
49	5.2	41.0	0.0121	0.0083
50	10.1	36.8	0.0119	0.0093
52	13.3	32.2	0.0105	0.0099
53	22.1	24.2	0.0100	0.0114
55	26.7	19.3	0.0092	0.0119
57	30.4	16.3	0.0078	0.0115
58	34.6	14.2	0.0071	0.0117
60	35.4	13.9	0.0064	0.0119

Decreasing Humidity

% Relative Humidity	Left-hand peak area (arb. units)	Right-hand peak area (arb. units)	Left-hand peak width ($Å^{-1}$)	Right-hand peak width ($Å^{-1}$)
56	36.0	11.7	0.0043	0.021
54	34.1	9.7	0.0052	0.018
53	31.1	11.5	0.0066	0.015
51	30.8	15.7	0.0094	0.0142
49	16.3	27.2	0.0141	0.0116
46	13.5	32.7	0.017	0.0101
44	11.4	36.5	0.020	0.0083
42	9.9	37.3	0.019	0.0075

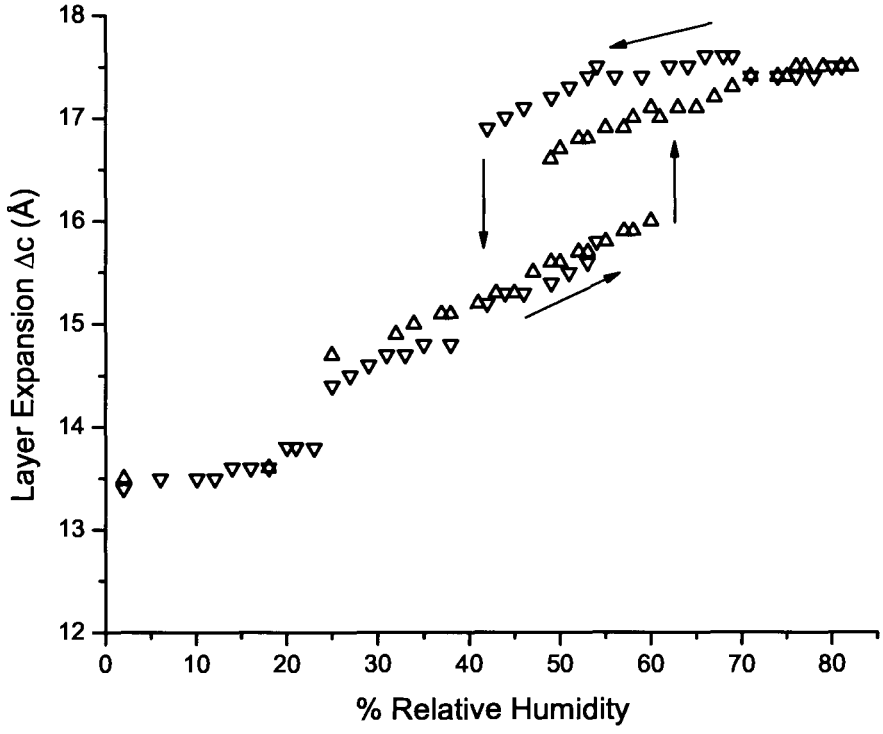

Figure 6.8: Expansion of plane spacing for phase A of Figs. 6.2 and 6.3 as a function of relative humidity. Triangles pointing up are for increasing humidity, and triangles pointing down are for decreasing humidity.

Fig. 6.8 clearly demonstrates the different size of the jump in spacing for the increasing and decreasing humidities. It also shows the hysteresis in the phase transition region, where the transition begins at higher humidity on the way up, and at lower humidity on the way down.

The coexistence of two phases over a significant range of humidity can be seen in the data and in Fig. 6.8. This coexistence is probably due to a small energy barrier existing between one phase and the other, and one phase being metastable in the region where the other should dominate. For example, as the humidity increases beyond around 50%, it appears that the higher-spacing phase is favoured. The survival of the low-spacing phase well beyond 50% RH can be explained by that phase being metastable above 50%, and needing to overcome a barrier to reach the more stable

phase. This sort of behaviour is consistent with a first-order phase transition.

The exact nature of this phase transition is not known, but presumably as enough water enters the system, the conformation of CMP changes to partially accommodate the additional water, though enough water gets near the interface that the layers are forced apart. The change in conformation could be the result of a rotation coupled with a partial insertion of water. What is clear is that there is a distinct shift in spacing, meaning that there are two stable conformations, and that the system is jumping from one to the other. It is worth noting that at high humidity, the peaks are narrowed, implying that the CMP-water system is better ordered within the layers than at low humidity.

The difference between the size of the jump on the way up and on the way down most likely arises because of the sample not having fully reached equilibrium on the increasing humidity side. Subsequent experiments with other samples of $Cd_{0.85}PS_{2.7}(CMP)_{0.3}$ in the 50-80 % RH range suggest that this difference is not significant when the sample is allowed to reach equilibrium over a period of hours, instead of the typical 20-30 minutes for the studies shown here. These findings imply that the difference in the high-spacing phase, as seen in the 50-70 % RH region of Fig. 6.8, is a kinetic effect, where the transformation has not been completed in the time alloted when taking the data. This is different from the main hysteresis curve in the area of 40-60 % RH, where there is a true phase transition.

While an electron density calculation might provide some guidance with respect to the conformation of the guest CMP molecules, it is difficult to perform such a calculation given that the peaks from different phases tend to overlap, which makes some of the peak intensities difficult to distinguish.

It should be pointed out that Sugawara *et al.* [30] have investigated a humidity-induced phase transition of crystalline Na_2CMP by X-ray diffraction. They observed four distinct phases, and the primary transition that they studied, which occurred around 50 % RH, displayed hysteresis, like the transition observed in this work. Their proposed model for the phase transition concerned interactions between the Na^+ ions, phosphate groups, and bridging water molecules. The authors mention that in this case, the CMP molecules shift in a cooperative manner such that the crystal does not crack. The similarities with the $CdPS_3$ system are minimal, but their work is an interesting example of the ability of the CMP molecules to shift their orientation and

conformation in order to accommodate changes in hydration.

Chapter 7

Discussion and Conclusions

7.1 Differences between $Cd_{0.85}PS_{2.7}(AMP)_{0.5}$ and $Cd_{0.85}PS_{2.7}(CMP)_{0.3}$ compounds

There are a number of differences between the $Cd_{0.85}PS_{2.7}(AMP)_{0.5}$ and $Cd_{0.85}PS_{2.7}(CMP)_{0.3}$ compounds, including their response to changes in relative humidity. In addition, a discussion of the difference in NMP/$CdPS_3$ ratio will be presented, as well as some comments on the ability of AMP to intercalate into $K_{0.4}Cd_{0.8}PS_3(H_2O)_y$, which was not observed for CMP.

7.1.1 Response to humidity

The different response of $Cd_{0.85}PS_{2.7}(AMP)_{0.5}$ and $Cd_{0.85}PS_{2.7}(CMP)_{0.3}$ to changes in RH are worth exploring at this point. The minimal response of the AMP system to humidity below 80 %, versus the more dramatic response of the CMP system, including a phase transition near 50 %, is notable. As mentioned in the introduction, it is well known that adenine is more hydrophobic than cytosine. Even during sample preparation, the AMP had to be heated in order to dissolve, while the CMP dissolved much more readily. Thus it appears that it is the base interactions with water which influence the change in host plane spacings, and not the hydrophilic phosphate groups. The presence of Li^+ may account for this in part, since it seems that the lithium ions become associated with the phosphate groups without a hydration shell, as suggested

in the study by Tajmir-Riahi and Messaoudi [29]. Therefore the phosphate groups are in a sense tied up by the Li^+, and not as free to accept water molecules, particularly in the direction that would expand the host layers. Instead, it is the hydrophilic sites of the bases that are available and cause the expansion of the layers due to bonding with water. The model given in chapter 4 for $Cd_{0.85}PS_{2.7}(AMP)_{0.5}$ is in agreement with this picture of particular base sites bonding in some way with water ahead of the phosphate group.

The steady increase in spacing with RH oserved in the $Cd_{0.85}PS_{2.7}(CMP)_{0.3}$ samples may be caused by increased water associating with ribose (sugar) OH groups and O or OH in the phosphate groups, but in a direction that is mostly parallel to the host basal planes. The water molecules would have a tendency to expand the layers only slightly since they are finding space to fill that is not directly at either end of the guest NMP, in other words not right at the interface with the host planes.

7.1.2 Differences in composition

Another difference between the two types of samples is the composition. As discussed in Chapter 3, the molar ratio of CMP to host unit is found to be about 0.3, and the ratio of AMP to host is 0.5. These findings are counter-intuitive, since AMP is a larger molecule, and one would expect, as a first guess, for an equal density of guest/host, a smaller ratio for AMP as compared to that of CMP. On the other hand, if we assume that each NMP molecule is associated with a positively charged site in the host (i.e. Li^+ ions near Cd vacancy sites), then one would expect the same occupancy for both CMP and AMP. For example, if we assume that the x value of lithium in $Li_xCd_{0.85}PS_{2.7}(CMP)_{0.3}(H_2O)_y$ is 0.35, in agreement with the findings of Lagadic *et al.* [32], then we would expect the same 0.35 value for the ratio of NMP to host unit. In neither simple case do we expect AMP to be more densely packed.

It is useful to compare the results of this work to the layered double hydroxide work of Choy *et al.* [2] and Lotsch *et al.* [6], in order to see what compositions were obtained for the other known examples of AMP and CMP included in layered compounds. The compositions found for the $CdPS_3$ systems is compared to those of the layered double hydroxide systems in Table 7.1.

It is interesting to note the variations in compositions among the three sets of

Table 7.1: Compositions of intercalated NMP samples into layered hosts.

Reference	Composition
Choy *et al.* [2]	$Mg_{0.66}Al_{0.34}(OH)_2(AMP)_{0.14}(OH)_{0.20}{\cdot}0.9H_2O$
"	$Mg_{0.66}Al_{0.34}(OH)_2(CMP)_{0.19}(OH)_{0.14}{\cdot}0.7H_2O$
Lotsch *et al.* [6]	$Li_{0.74}Al_2(OH)_6(AMP)_{0.37}{\cdot}2.2H_2O$
"	$Li_{0.23}Al_2(OH)_6(CMP)_{0.12}{\cdot}0.9H_2O$
Present work	$Li_xCd_{0.85}PS_{2.7}(AMP)_{0.5}(H_2O)_y$
"	$Li_xCd_{0.85}PS_{2.7}(CMP)_{0.3}(H_2O)_y$

data. Lotsch's work agrees with the present work in that AMP appears to be more densely arranged than CMP within the layers, but Choy's work does not show the same trend.

One possible reason for which more AMP would be present than CMP is that the mainly hydrophobic adenine bases may be stacking partially to avoid contact with water, allowing the AMP to pack more closely together. The greater hydrophilicity of CMP would then prevent the same sort of base stacking from occurring with CMP.

A greater density of AMP molecules within the host layers could also contribute to the lack of significant change in layer spacing with humidity for the AMP samples, while the converse is true for CMP. A lower density allows more space for water molecules to enter the interlayer region.

7.1.3 Intercalation of NMPs into $K_{0.4}Cd_{0.8}PS_3(H_2O)_y$

As shown in Chapter 5, AMP was found to intercalate into $K_{0.4}Cd_{0.8}PS_3(H_2O)_y$, while CMP intercalation was unsuccessful. A reason for this difference is related to the different hydrophobicities of AMP and CMP. Since AMP is more hydrophobic, it is perhaps more energetically favourable to enter the layers in order to avoid being in solution.

In their LDH/NMP work, Lotsch *et al.* [6] investigated the preferential intercalation of combined solutions of NMPs into LDH hosts. They found that for a wide selection of LDH materials, CMP intercalated preferentially at a ratio of about 70-80 % over AMP. It would be interesting to attempt this with a combined solution of CMP and AMP in MPS_3 materials and to quantify the results.

7.2 Na_2AMP and Na_2CMP

Attempts to form restacked inclusion compounds with solutions of Na_2AMP and Na_2CMP were not successful. It appears that the Na^+ ions were exchanged for the Li^+ within the layers, and immediate flocculation of the suspension was observed, forming a powder with a spacing that corresponded to the water bilayer system observed for $CdPS_3$ intercalated with Na or Li [34].

This observation fits in with the discussion above, where it is thought that the NMP molecules are included within the layers in their neutral form, since as negative ions they would be repelled by the partially negatively charged $Cd_{0.85}PS_{2.7}$ layers [11]. The neutral form in this case consists of a protonated N atom in the base and a negatively charged phosphate, the same as is observed in the formation of H_2NMP crystals [26–28].

7.3 Phase transition of $Cd_{0.85}PS_{2.7}(CMP)_{0.3}$

There remain a few comments to be made on the phase transition discussed in Chapter 6, based on the XRD data of Figs. 6.2 and 6.3. In the analysis of the peak positions and widths, it was mentioned that the domains of one phase are reduced in size as the other phase increases. An illustration of what a particle may look like while two distinct peaks are observed is shown in Fig. 7.1.

The diagram shows that as the humidity increases, water enters from the edge of the particle, forcing the phase transition to occur. Thus domains are formed where part of the particle is still in the old phase, while the other part is in the new phase.

The data rule out the possibility of ordered staging, in which, for example, every second layer undergoes the phase transition first, followed by the others. If staging were to occur, new XRD peaks would appear due to the formation of a superlattice. A diagram showing staging is given in Fig. 7.2.

A schematic depiction of what may be occurring inside the layers before and after the phase transition is shown in Fig. 7.3. The phosphate groups, represented by an encircled P in the top picture, are bonded to the Li^+ site. The empty space between CMP molecules is gradually filled with water molecules, represented by W in the diagram. Eventually, the empty space gets filled, and as new water molecules enter

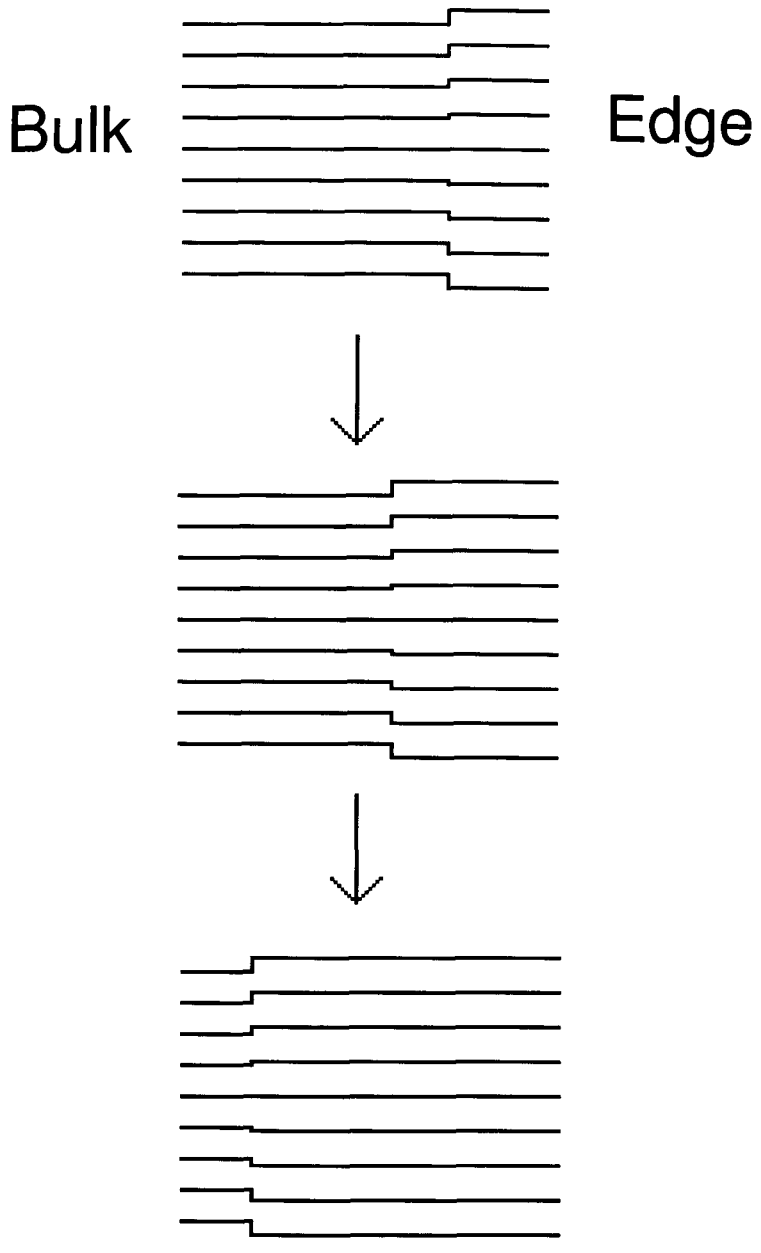

Figure 7.1: Schematic depiction of the phase transition in $Cd_{0.85}PS_{2.7}(CMP)_{0.3}$, showing the formation of distinct domains in a given particle as water enters from (or exits through) the edge.

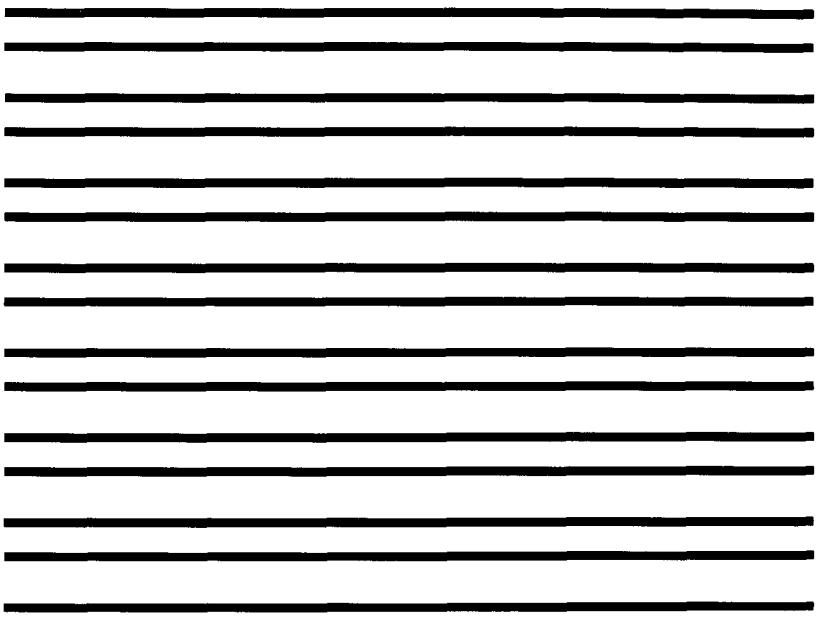

Figure 7.2: Schematic depiction of an ordered staging process, where every second interlayer space undergoes an expansion.

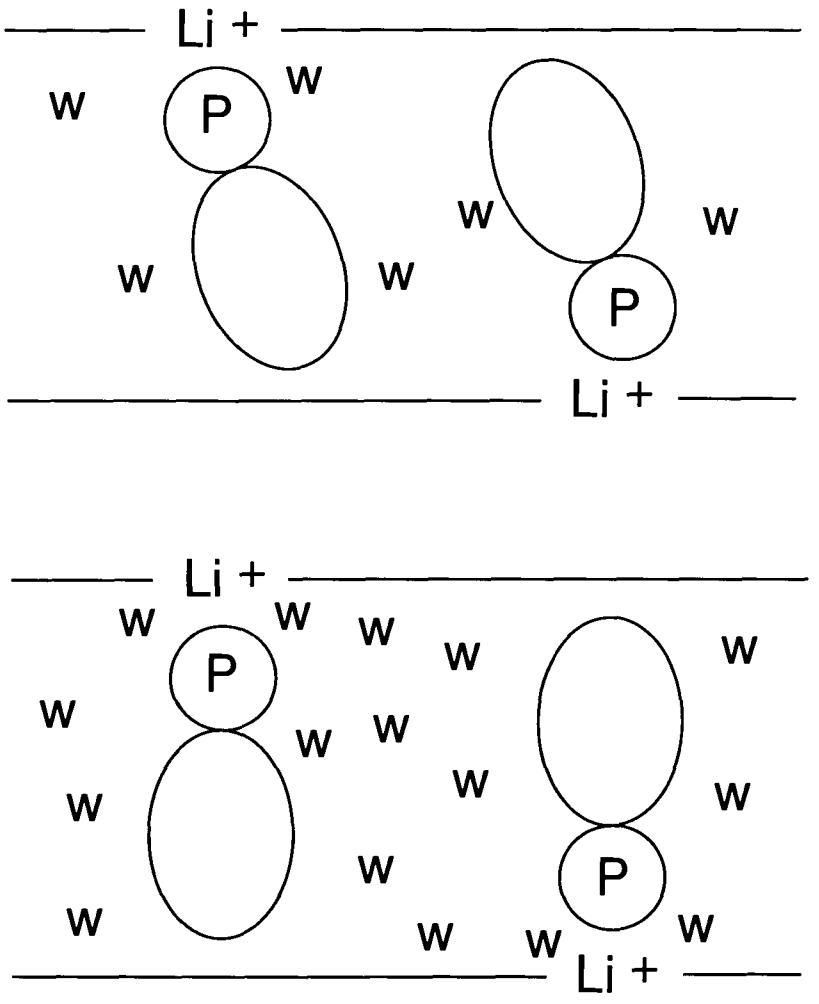

Figure 7.3: Schematic depiction of the phase transition in $Cd_{0.85}PS_{2.7}(CMP)_{0.3}$, showing the expansion of the layers as increased water and a change in CMP conformation force the layers apart. W represents water molecules, the P surrounded by a circle represents the phosphate group, and the large oval represents the base + sugar.

the system, they may cause the CMP molecule to rotate or shift in some way, allowing the water molecules partial access to the phosphate-Li region and forcing the layers apart. This situation is shown in the bottom picture of Fig. 7.3.

The exact mechanism for this change, and the reasons for which it is occurring in the CMP system but not in AMP, are not known for certain. Nevertheless, some possibilities are presented here. It appears that a sudden change in conformation is occurring within the CMP molecule. One possible changes would be a modification of the conformation of the base, moving to the *anti* position, in which the base is as depicted in Fig. 1.6, spread out away from the sugar and phosphate, from the *syn* position, in which the base is closer to the phosphate, and over the sugar. This would increase the size of the CMP molecule in a sudden way consistent with the observed phase transition. According to Saenger [19] and references therein, all 5′ NMPs are found in the *anti* conformation in solution and in solid form. However, when the phosphate group is not present, cytidine is found equally in the *anti* and *syn* conformations, while adenosine prefers the *anti* conformation. This could help to account for the lack of a phase change noted for the AMP system in this thesis. It is also noted that the presence of ions can change the affinity for *syn* or *anti* conformation in NMPs. I could not find a study in which the effects of hydration on the conformation of NMPs suggested that this change in the conformation of CMP is expected, but the fact that the molecule is confined in two dimensions could help make the *syn* conformation more likely at low humidity.

Another conformational change that can occur in NMPs is a change in the sugar puckering state. The sugar ring is not planar, but is puckered, generally with either the C2′ or the C3′ atom sticking out from the plane. A change from one to the other has been observed in many situations, sometimes related to humidity. While this change alone would not account for a significant change in molecule size, it could facilitate the *syn* - *anti* conformational change, as has been shown for nucleosides (NMPs without the phosphate) [19].

7.4 Conclusions and future directions

The inclusion of AMP and CMP into $CdPS_3$ was presented and explored in this work. Among the features found were significant differences in the responses of the

hybrid layered compounds to humidity, where the CMP samples underwent a phase transition and the layer spacing varied by about 4 Å over the humidity range studied (0-80%). A model was presented for the $CdPS_3$/AMP system based on electron density calculations and other considerations. It was also found that the acid form of the molecules was able to form restacked composites, while the ionic salt forms were not, due to repulsion with the negatively charged host layers.

It was found that the difference in hydrophobicity of the two molecules affects the properties of the inclusion compounds. Both the difference in response to humidity as well as the ability of AMP to intercalate into K^+-intercalated $CdPS_3$ while CMP could not, are examples of these differences.

The electron density calculations also suggest that there is a buckling in the host layers of ± 0.6 Å, which has not been observed or discussed previously in MPS_3 materials. This observation could be confirmed or modified by an investigation using X-ray Absorption - Fine Spectrum analysis, where the local atomic bond lengths of the host layers could be determined.

The phase transition that was found for the $CdPS_3$/CMP samples could be explored further with humidity-controlled Infrared Spectroscopy. This method could help sort out the differences in guest CMP conformation below and above the phase transition, by noting the changes in the hydrogen bonding of the molecule. In addition, the water content for both the AMP and CMP systems can be found using thermal gravimetric analysis, where the samples would be weighed with heating, or perhaps a gravimetric analysis where only the humidity is varied. In the thermal case, the initial humidity would have to be well controlled in order to properly correlate water content to the basal plane spacings found by X-ray diffraction.

In addition, it should be possible to determine whether or not the CMP conformation is changing from *syn* to *anti*, and understanding the nature of the differences with AMP, by trying the same experiments with different NMPs. If size is a determining factor, then inosine monophosphate (IMP) and guanosine monophosphate (GMP) should show the same behaviour as AMP, since they are all of similar size, while uridine monophosphate (UMP) would behave as CMP does. In addition, GMP has a stronger affinity for water than AMP does, so experiments with GMP should help sort out whether hydrophilicity is important in the phase transition behaviour.

Other future directions that these studies could take would be to perform exper-

iments with other layered host systems and compare the CMP and AMP densities and conformations with those that have alrady been found. This would help to determine what properties are independent of the layered host chosen, and what properties are the same for all confined conditions. For example, it would be useful to clarify the wide variety of molar ratios found for AMP/host and CMP/host systems and to determine whether there truly is a tendency for AMP to pack more densely.

Bibliography

[1] G. Ouvrard, R. Brec, and J. Rouxel. Structural determination of some MPS_3 layered phases (M = Mn, Fe, Co, Ni and Cd). *Mat. Res. Bull.*, 20:1181–1189, 1985.

[2] J.-H. Choy, S.-Y. Kwak, J.-S. Park, Y.-J. Jeong, and J. Portier. Intercalative nanohybrids of nucleoside monophosphates and DNA in layered metal hydroxide. *J. Am. Chem. Soc.*, 121:1399–1400, 1999.

[3] J.-H. Choy, J.-S. Park, S.-Y. Kwak, Y.-J. Jeong, and Y.-S. Han. Layered double hydroxide as gene reservoir. *Mol. Cryst. Liq. Cryst.*, 341:425–429, 2000.

[4] J.-H. Choy, S.-Y. Kwak, Y.-J. Jeong, and J.-S. Park. Inorganic layered double hydroxides as nonviral Vectors. *Angew. Chem. Int. Ed.*, 39(22):4041–4045, 2000.

[5] J.-H. Choy, S.-Y. Kwak, J.-S. Park, and Y.-J. Jeong. Cellular uptake behavior of [$\gamma-^{32}$P] labeled ATP-LDH nanohybrids. *J. Mater. Chem.*, 11:1671–1674, 2001.

[6] B. Lotsch, F. Millange, R. I. Walton, and D. O'Hare. Separation of nucleoside monophosphates using preferential anion exchange intercalation in layered double hydroxides. *Solid State Sciences*, 3:883–886, 2001.

[7] T. Coradin, A. Coupé, and J. Livage. Intercalation of biomolecules in the $MnPS_3$ layered phase. *J. Mater. Chem.*, 13:705–707, 2003.

[8] P. Westreich, D. Yang, and R. F. Frindt. The encapsulation of nucleoside monophosphates into $Cd_{0.8}PS_3$. *J. Phys. Chem. Solids*, 65:583–586, 2004.

[9] S.-Y. Kwak, Y.-J. Jeong, J.-S. Park, and J.-H. Choy. Bio-LDH nanohybrid for gene therapy. *Solid State Ionics*, 151:229–234, 2002.

[10] S.-Y. Kwak, S.-H. Hwang, Y.-J. Jeong, J.-S. Park, and J.-H. Choy. Insertion of inorganic-biomolecular nanoyhybrid into eucaryotic cell. *Mat. Res. Soc. Symp. Proc.*, 703:V13.44.1–V13.44.6, 2002.

[11] D. Yang, P. Westreich, and R. F. Frindt. Exfoliated $CdPS_3$ single layers and restacked films. *J. Solid State Chem.*, 166:421–425, 2002.

[12] A. I. Khan and D. O'Hare. Intercalation chemistry of layered double hydroxides: recent developments and applications. *J. Mater. Chem.*, 12:3191–3198, 2002.

[13] R. Clément. A novel route to intercalation into layered $MnPS_3$. *J. Chem. Soc. Chem. Commun.*, pages 647–648, 1980.

[14] V. Grasso and L. Silipigni. Low-dimensional materials: The MPX_3 family, physical features and potential future applications. *Rivista del Nuovo Cimento*, 25 (6):1–102, 2002.

[15] R. Clément, O. Garnier, and J. Jegoudez. Coordination chemistry of the lamellar MPS_3 materials: Metal-ligand cleavage as the source of an unusual "cation-transfer" intercalation process. *Inorg. Chem.*, 25:1404–1409, 1986.

[16] J. S. O. Evans, D. O'Hare, and R. Clément. The structure of $Co(\eta\text{-}C_5H_5)_2{}^+$ and NMe_4+ intercalates of $MnPS_3$: An X-ray, neutron-diffraction, and solid-state NMR study. *J. Am. Chem. Soc.*, 117:4595–4606, 1995.

[17] J. Schmedt auf der Günne, H. Eckert, A. Léaustic, and F. Babonneau. Vacancy ordering and host-guest interactions in $CdPS_3$ intercalates: Results from multi-dimensional solid state NMR. *Phys. Chem. Chem. Phys.*, 5:1306–1313, 2003.

[18] R. F. Frindt, D. Yang, and P. Westreich. Exfoliated single molecular layers of $Mn_{0.8}PS_3$ and $Cd_{0.8}PS_3$. Submitted to *J. Mater. Res.* on Sept. 24, 2004.

[19] W. Saenger. *Principles of Nucleic Acid Structure.* Springer-Verlag, New York, 1984.

[20] J. D. Watson and F. H. C. Crick. Molecular structure of nucleic acids: A structure for deoxyribose nucleic acid. *Nature*, 171:737–738, 1953.

[21] R. E. Franklin and R. G. Gosling. The structure of sodium thymonucleate fibres. I. The influence of water content. *Acta. Cryst.*, 6:673, 1953.

[22] S. Ganguly and K. K. Kundu. Transfer energetics of uracil, thymine, cytosine and adenine in aqueous mixtures of lithium chloride, sodium chloride and potassium chloride. *Indian J. Chem. A*, 34:857–865, 1995.

[23] P. Shih, L. G. Pedersen, P. R. Gibbs, and R. Wolfenden. Hydrophobicities of the nucleic acid bases: Distribution coefficients from water to cyclohexane. *J. Mol. Biol.*, 280:421–430, 1998.

[24] R. Schneider, D. Cohen, and H. M. Berman. Hydration of DNA bases: Analysis of crystallographic data. *Biopolymers*, 32:725–750, 1992.

[25] A. Shestopalova. Hydration of nucleic acid components in dependence on nucleotide composition and relative humidity: A Monte Carlo simulation. *Eur. Phys. J. D*, 20:331–337, 2002.

[26] J. Kraut and L. H. Jensen. Refinement of the crystal structure of adenosine-5'-phosphate. *Acta Cryst.*, 16:79–88, 1963.

[27] M. Sundaralingam and L. H. Jensen. Stereochemistry of nucleic acid constituents I. Refinement of the structure of cytidylic acid b. *J. Mol. Biol.*, 13:914–929, 1965.

[28] M. Sundaralingam and L. H. Jensen. Stereochemistry of nucleic acid constituents II. A comparative study. *J. Mol. Biol.*, 13:930–943, 1965.

[29] H.-A. Tajmir-Riahi and S. Messaoudi. The Effects of Monovalent Cations Li^+, Na^+, K^+, NH_4^+, Rb^+ and Cs^+ on the Solid and Solution Structures of the Nucleic Acid Components. Metal Ion Binding and Sugar Conformation. *J. Biomol. Struct. Dyn.*, 10(2):345–365, 1992.

[30] Y. Sugawara, A. Nakamura, Y. Iimura, K. Kobayashi, and H. Urabe. Crystallographic investigation of humidity-induced phase transition of disodium cytidine 5'-monophosphate and crystal structure of three hydrates. *J. Phys. Chem. B*, 106:10363–10368, 2002.

[31] J. Covino, P. Dragovich, C. K. Lowe-Ma, R. F. Kubin, and R. W. Schwartz. Synthesis and characterization of stoichiometric $CdPS_3$. *Mat. Res. Bul.*, 20: 1099–1107, 1985.

[32] I. Lagadic, P. G. Lacroix, and R. Clément. Layered MPS_3 (M = Mn, Cd) thin films as host matrixes for nonlinear optical material processing. *Chem. Mater.*, 9:2004–2012, 1997.

[33] L. Reimer. *Scanning Electron Microscopy.* Springer, New York, 2nd ed., 1998.

[34] P. Jeevanandam and S. Vasudevan. Preparation and characterization of $Cd_{0.75}PS_3A_{0.5}(H_2O)_y$ [A = Na, K and Cs]. *Solid State Ionics*, 104:45–55, 1997.

[35] N. Arun, S. Vasudevan, and K. V. Ramanthan. Orientation and motion of interlamellar water: An infrared and NMR investigation of water in the galleries of layered $Cd_{0.75}PS_3K_{0.5}(H_2O)_y$. *J. Am. Chem. Soc.*, 122:6028–6038, 2000.

[36] B. D. Cullity. *Elements of X-Ray Diffraction.* Addison-Wesley, Don Mills, 2nd ed., 1978.

[37] R. A. Gordon, D. Yang, E. D. Crozier, D. T. Jiang, and R. F. Frindt. Structures of exfoliated single layers of WS_2, MoS_2, and $MoSe_2$ in aqueous suspension. *Physical Review B*, 65:125407, 2002.

[38] A. Guinier. *X-ray Diffraction in Crystals, Imperfect Crystals, and Amorphous Bodies.* Dover Publications Inc., New York, 1994.